12-2004

Combinatorial Design of Nickel-Chromium Alloys By Physical Vapor Deposition And Electron Beam Welding

Jaret James Frafjord
University of Tennessee - Knoxville

To the Graduate Council:

I am submitting herewith a thesis written by Jaret James Frafjord entitled "Combinatorial Design of Nickel-Chromium Alloys By Physical Vapor Deposition And Electron Beam Welding." I have examined the final electronic copy of this thesis for form and content and recommend that it be accepted in partial fulfillment of the requirements for the degree of Master of Science, with a major in Materials Science and Engineering.

George M. Pharr, Major Professor

We have read this thesis and recommend its acceptance:

Easo P. George, Phillip D. Rack

Accepted for the Council:
Carolyn R. Hodges

Vice Provost and Dean of the Graduate School

(Original signatures are on file with official student records.)

To the Graduate Council:

I am submitting herewith a thesis written by Jaret James Frafjord entitled "Combinatorial Design of Nickel-Chromium Alloys By Physical Vapor Deposition And Electron Beam Welding." I have examined the final electronic copy of this thesis for form and content and recommend that it be accepted in partial fulfillment of the requirements for the degree of Master of Science, with a major in Materials Science and Engineering.

George M. Pharr

George Pharr, Major Professor

We have read this thesis and
recommend its acceptance:

Easo P. George

Phillip D. Rack

Acceptance for the Council:

Anne Mayhew

Vice Chancellor and
Dean of Graduate Studies

(Original signatures are on file with official student records.)

Combinatorial Design Of Nickel-Chromium Alloys By Physical Vapor Deposition And Electron Beam Welding

A Thesis
Presented for the
Masters of Science
Degree
The University of Tennessee, Knoxville

Jaret James Frafjord
December 2004

Dedication

This thesis is dedicated to my parents, Michelle & Curt Wittreich and Dean & Janene Frafjord, who always believed in me, encouraged me to work harder than the rest, and inspired me to perform to the best of my abilities.

This is also dedicated to my siblings, Karissa Jacobson, Monica Wittreich, Tyler Wittreich, and Kristen Frafjord, and the rest of my family for all of their support and encouragement.

Acknowledgements

I wish to thank all of those who helped me in completing my Master of Science degree in Materials Science and Engineering. I would like to thank Dr. Yang-Ki Hong at the University of Idaho for encouraging me to work hard always and pressing me to continue my education. I would like to thank Dr. George Pharr at the University of Tennessee for his guidance and support through both the positive and frustrating results obtained during the research for this thesis. I must also show appreciation to Dr. Easo George and Dr. Phillip Rack for serving on my committee.

I would like to thank Dr. Mike Santella at ORNL for his efforts to ensure that I learned more than I ever thought I would. I must thank Alan Frederick at ORNL for his help and understanding with the PVD and EBW systems, Dr. Andrei Rar for his help with nanoindentation, and Dr. Hongbin Bei for his help with the cast standards. A special thanks to Tom Geer at ORNL for all of his help with metallography and for his genuine concern with my advancement in life. I would like to also thank Dr. Dongyun Lee for his help with microscopy, and for his encouragement that kept me motivated toward the end.

I need to thank my family and several lifelong friends, namely Erica Paulson, for their love, motivation, and encouragement through the end. Lastly, I would like to thank my friends in Knoxville, namely Steve Russell, for keeping my sanity intact and for making my transition to the SEC a wonderful experience.

Abstract

Combinatorial methods, which include high efficiency and high throughput methods to create a large compositional range of materials, have proven to be highly effective and efficient in research and development in the chemical and pharmaceutical industries. In this thesis, similar methods for the development and optimization of metals and alloy systems are explored. Combinatorial Ni-Cr alloy samples were developed by physical vapor deposition (PVD) of a wedged film on a bulk material, and then locally melting the two by electron beam welding (EBW). A combinatorial alloy gradient was thus created along the length of the weld. The samples were rapidly characterized for chemical properties by energy dispersive x-ray spectrometry (EDS) and for mechanical properties, namely modulus and hardness, by nanoindentation. All measurements were compared with similar tests on melted and cast Ni-Cr alloy standards, and the microstructures were compared by scanning electron microscopy (SEM).

The entire Ni-Cr composition range was established and reproduced with several welded samples of both nickel films on chromium substrates and chromium films on nickel substrates. There were no strong tendencies in the elastic modulus measurements compared to composition, though all values were within reasonable deviation of the modulus of the cast standards. On the other hand, there were strong trends in the hardness measurements that followed similar tendencies of the standard cast Ni-Cr alloys. The hardness values also showed trends that coincided with the composition and phases associated with the Ni-Cr phase diagram. The hardness results obeyed a more definite trend in the nickel rich γ-phase, where the hardness increased linearly from 1.2 GPa at pure nickel to about 3.5 GPa at 40 at% Cr. The hardness of the chromium rich α-phase approached nearly 13 GPa when the alloy was between 70 and 85 at% Cr, and then dropped toward the hardness of pure chromium at 3.7 GPa.

Table of Contents

List of Figures

Chapter 1: Introduction

Combinatorial methods include high efficiency and high throughput methods to create a large compositional range of materials, or "composition libraries" [4]. These continuous compositional samples are then tested systematically for rapid characterization of the properties of interest. Combinatorial science "is an approach to the discovery and study of new materials that combines rapid chemical synthesis, high throughput screening, and high-capacity information processing to rapidly create, analyze, and interpret enormous numbers of new and diverse material compositions" [2]. This method is far more efficient and effective than the time consuming conventional process of testing one composition at a time.

In principle, the methodology of combinatorial chemistry is quite simple: two or more chemical species are systematically combined in various proportions, and the properties of each of the resulting combinations are assessed to identify those with unique or desirable characteristics. Recent advances in the field have been made possible by the development of automated processes for producing large numbers of chemical compounds in convenient miniature arrays and techniques for rapidly assessing their properties.

The high-throughput screening for new drugs and biomolecules that is now possible with the help of combinatorial chemistry has already revolutionized the pharmaceutical and biotechnology industries [1-3]. In fact, all major pharmaceutical companies are now using combinatorial methods to accelerate the discovery and optimization of new drugs [5]. While these examples of the successful use of combinatorial techniques are all limited to organic and inorganic chemistry, there is increasing interest in applying the basic principles of high-throughput and combinatorial techniques in the search for, and optimization of, new materials in other fields.

In the 1990's, materials scientists adopted these combinatorial methods to search for and optimize new engineering materials for a wide variety of applications [1-2]. Although still in its infancy, combinatorial materials science has been successfully employed to discover a host of new materials for photoluminescence, catalysis, and superconductivity, as well as for applications as dielectric, magnetic, and ferroelectric materials [1-3].

According to a recent "Research News" article in the journal *Science* [12], further advances in this area will benefit a whole host of U.S. industries. In this context, it is notable that the Materials Research Society held its first ever symposium in this area at the Fall 1998 meeting and followed it up with a second symposium at the Fall 2001 meeting. As pointed out in the symposium announcements, combinatorial approaches, artificial intelligence methods, and other high-throughput techniques are emerging that will increase the efficiency with which new materials and processes are discovered and improved.

Combinatorial Methods for Alloy Design

The basic principles of combinatorial chemistry have much to offer in the field of alloy design. For example, current techniques for preparing metallic alloys unavoidably restrict us to narrow ranges of alloy composition. Combinatorial methods promise to enhance significantly the composition range that can be explored, thereby leading to the discovery of important new materials. Combinatorial methods will also be useful in optimizing existing alloys. Because of the time and expense of qualifying engineering materials, the industrial approach often is to tweak existing alloys to improve their properties rather than to develop new alloys from scratch.

An example of a conventional industrial approach to alloy optimization at the Oak Ridge National Laboratory (ORNL) is work with Teledyne Allvac on phosphorous and boron additions in alloy 718 and Waspaloy to improve creep-rupture properties [7]. Another example is of ORNL's work with Siemens-Westinghouse on control of zirconium, boron,

and sulfur in Inconel-939 to improve its weldability for use in land-based gas turbines. ORNL also has ongoing work with Ford and Wescast to modify the composition of ductile cast iron so that it can be used at higher temperatures in next-generation exhaust manifolds. In all of these alloy optimization projects, the combinatorial approach would be an invaluable screening tool that could dramatically shorten the time necessary to investigate the various alloy compositions. Also, a wider range of composition space could be explored, possibly leading to better alloys.

To realize its full potential as a materials research tool, the combinatorial methodology has to address not just chemical composition but also processing issues. In many engineering applications the microstructure produced by a specific processing method has just as much of an influence on properties, if not more, than the chemical composition. Therefore, it is necessary to produce combinatorial samples that retain a microstructure equivalent to that produced from conventional processes. In this regard, there is a critical difference between combinatorial materials science and combinatorial chemistry.

There are numerous scientific advances that must be made in each of these areas before the potential of combinatorial alloy design can be fully realized. Clearly, the first step in this process is the production of suitable samples that can be rapidly and inexpensively produced in convenient forms for rapid testing. What is needed to apply combinatorial methods to alloy design and optimization are simple methods for making alloys in a variety of compositions, and equally simple methods for rapidly assessing the structure and the properties of the large number of combinations which must be explored.

Economic Advantages

Advancements in combinatorial methods will provide an economic advantage to industries involved with alloy design. Present combinatorial successes in the chemical and pharmaceutical industries have proven how these methods can reduce time, energy, and costs in the development and discovery of new materials. Compared to the

conventional one at a time approach of alloy design, combinatorial methods offer a reduction in material cost and supply, reduced development and processing time, less energy and cost associated with melting material, and fewer man hours required of technical personnel.

In an interview of thirty experts from the plastic industry, it was estimated that combinatorial methods would shorten the time in research and development by one year and shorten the time spent in pilot production by another year. It was also estimated that this would allow for a 15% price premium due to the product being introduced to the market so much earlier [5].

In a collaborative study of chemical industries, it was estimated that combinatorial methods could potentially shorten the discovery phase of chemical and materials research from the current two to three years to the possible three to six months. These methods could also possibly reduce the development phase from the current two to five years to the potential six to twelve months [6].

Competition in the global market drives the need for cheaper and more efficient manufacturing technology and development. Products must have the highest quality and performance, and yet reach the market faster. There is also a desire to miniaturize parts and create multifunctional materials. As better equipment is established to produce and characterize combinatorial materials, and improved technology is integrated to analyze large quantities of data faster, companies will recognize combinatorial science as the driving force to improving productivity [6].

Contributions in Combinatorial Materials Design

There are numerous techniques for creating combinatorial material libraries. Ainissa Ramirez, at Agere Systems in New Jersey, used co-sputtering to simultaneously deposit two metals to create a combinatorial library in order to search for the optimal material for

switches in microelectromechanical devices. She used gold to provide the desired electrical properties and cobalt or antimony to strengthen the weak gold. She annealed the samples and tested for conductivity, as well as for mechanical properties by nanoindentation [8].

Xiao-Dong Xiang at Lawrence Berkeley Laboratory conducted research in superconducting materials by combinatorial methods. He sputtered layers of thin films using radio frequency magnetron sputtering through multiple physical masks to create thousands of combinations of metal oxides, and then diffused the layers by sintering in air. He found superconductivity in BiSrCaCuO and YBaCuO films at temperatures of 80 to 90 K, with surface areas as small as 200 μm by 200 μm and library densities of 10,000 sites per square inch [9].

Xiang has also used this technique, as well as another technique involving co-sputtering of multiple targets at once, to create continuous combinatorial libraries for mapping the electrical and magnetic properties of doped manganese oxides. After post annealing, he discovered several promising electronic characteristics in $La_{1-x}Ca_xMnO_3$ and $Nd_{1-x}Sr_xMnO_3$ materials. He noted that the synthesis and discrete characterization of the phase diagrams of these materials by conventional methods would have taken years due to the complicated growth of the single crystals used [10].

Combinatorial research at Symyx Technologies in California led to the discovery and optimization of several key luminescent materials. In 1998, the work produced a "bona fide" discovery of an unusual luminescent blue phosphor, Sr_2CeO_4. This material was found after making a combinatorial array by electron beam evaporation with multiple targets and moving masks. The properties of these thin films were equivalent to those achieved by bulk materials produced by conventional means [11-12].

There has been much research in applying combinatorial methods in materials design to characterize electrical and magnetic properties, but there has been little published

research aimed at characterizing mechanical properties of alloys by combinatorial methods. Some have tried using multiple thin films to incorporate composition gradients in specific materials. The two largest contributors to combinatorial alloy design have been from France and the United States.

A group in France proposed a combinatorial method for alloy design by a melting zone technique. They created a compositional gradient of aluminum and cobalt between 16 and 50 at% Co over a length of 7 cm. They began with a feed rod consisting of two parts with tilted interfaces as shown in Figure 1. Rod "A" had a composition of 50 at% Co, and rod "B" had a composition of 16 at% Co. The molten zone was created by induction heating at a speed of 7.5 cm per hour. They successfully observed all the different structures suggested by the phase diagram, and were also able to test mechanical properties by microhardness. They noted that this method can be used for any system over different compositional ranges, with the possibility of miniaturizing the sample size [13-14].

Ji-Cheng Zhao, of General Electric Company, has developed the most significant research program in combinatorial alloy design. He created a "diffusion multiple" that established diffusion gradients between four different bulk metals. These methods not only create a binary alloy system, but also ternary and quaternary systems [8,15-17]. He has proven this method for several different alloy systems, two of which are described below.

Figure 2 shows an example of Zhao's "diffusion multiple" of nickel, iron, molybdenum, and Inconel-706, with an outer diameter of 25 mm [15]. Zhao's diffusion multiple was created by machining pie-shaped and round shell-shaped high purity metals by electrical discharge machining (EDM). The five pieces were then joined together by hot isostatic pressing (HIP). This sample was annealed in vacuum at 1100ºC for 1500 hours to achieve suitable interdiffusion for analysis.

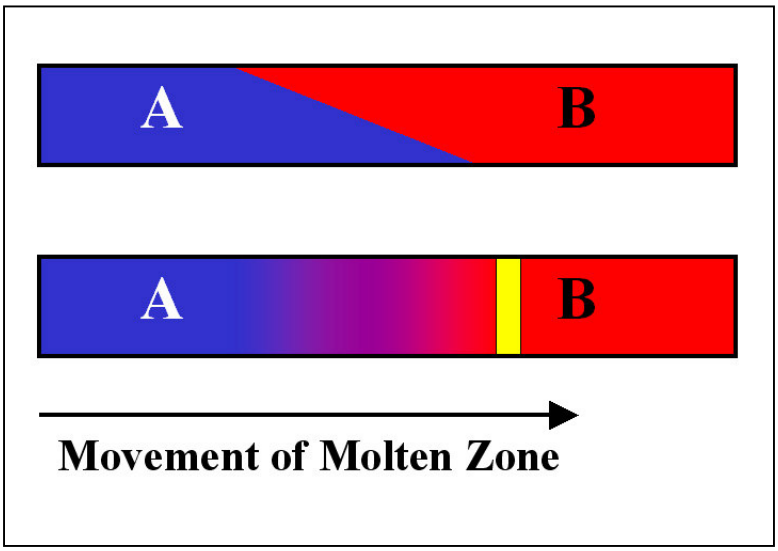

Figure 1: Combinatorial design by the molten zone technique.

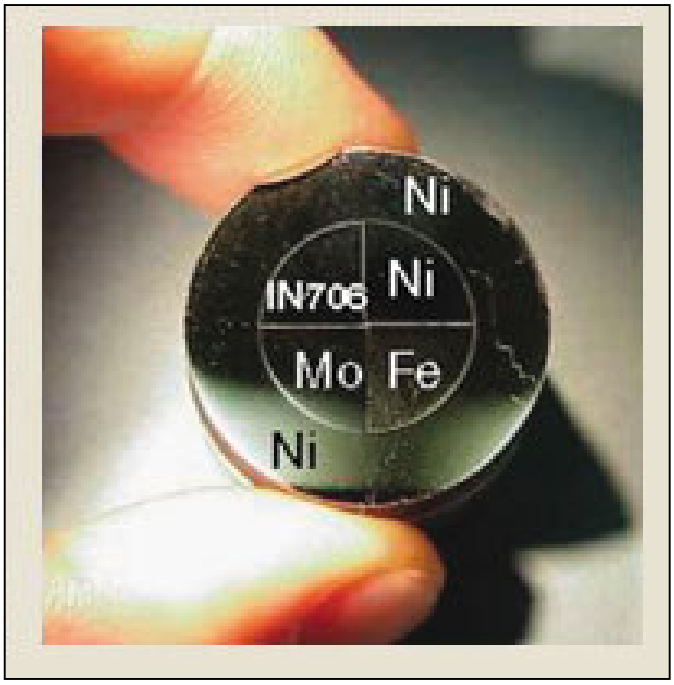

Figure 2: Zhao's "diffusion multiple" of Ni, Fe, Mo, and Inconel-706 [15].

He also produced a diffusion multiple of niobium, titanium, silicon, and chromium by the same methods as described above, with annealing in vacuum at 1000ºC for 4000 hours [17]. He used analytical tools such as the electron backscatter diffraction (EBSD) to determine crystal structure, electron probe microanalysis (EPMA) to determine composition profiles, and nanoindentation to establish mechanical properties.

Zhao's research has successfully led to the better understanding of several key ternary phase diagrams. He was able to create and prove that there are fourteen equilibrium phases within the Nb-Cr-Si ternary diagram [17]. His diffusion approach created the equilibrium conditions necessary for phase diagram development. Though this has proven an invaluable technique for determining the equilibrium phase diagrams, most industrial applications do not produce materials that reach complete equilibrium due to melting, casting, and annealing effects.

Objectives of This Project

The purpose of this project is to develop a methodology for designing and optimizing metallic alloys by combinatorial principles. The specific objectives of the research are: (1) to devise a simple means by which a test specimen with a library of alloy compositions spanning the range interest can be produced; (2) to assess how well the properties of the combinatorial specimen reproduce those of conventionally processed alloys; and (3) to devise screening tools which can be used to rapidly assess important alloy properties and identify optimum alloy compositions.

A new technique in combinatorial alloy design is developed that will produce alloys similar to those in industrial cast alloys. The methods do not use high temperature diffusion for alloying, and produce alloys that are in a non-equilibrium state similar to cast alloys. The methods have the potential to take far less time to produce a sample than those produced by diffusion. The samples will be useful in rapid characterization of an

alloy library where designers can narrow the compositional region search for the required mechanical properties of the desired alloy system.

As shown in Figure 3, the alloy libraries are made by vapor depositing thin wedged films of metal "A" on a substrate of metal "B", and then alloying by localized melting with a focused electron-beam welding (EBW) system. The e-beam welds run the length of the wedge to create a compositional gradient. The EBW technique creates melted and solidified alloys similar to those produced by conventional methods. The composition and properties of the specimens are assessed using EDS and nanoindentation.

Advantages of These Methods

Many researches believe that developing combinatorial alloys with thin films will not correlate well with similar alloys created by conventional means due to the inability to produce the desired microstructures [15]. This project uses thin films deposited on bulk material, and the melting of the two metals to create a microstructure similar to alloys created by conventional casting methods. By using a thin film as one of the alloy constituents, less material is needed to create a combinatorial sample than those samples using only bulk materials. This decrease provides reduced costs for sample preparation.

The samples produced by EBW techniques can be made in a very short amount of time. After a substrate is polished, it only takes about a day to deposit the necessary wedged film and only a few hours to make several e-beam welds across the length of the sample. In contrast, it can sometimes take months to establish suitable diffusion between bulk samples in order to create the necessary "alloy library" [15-17].

To date, most techniques for producing combinatorial alloy libraries have been based on diffusion multiples that give equilibrium structures. Alloys produced in industry are frequently not in the equilibrium state. Therefore, there are distinct advantages to samples made by welding that resemble cast alloys.

A

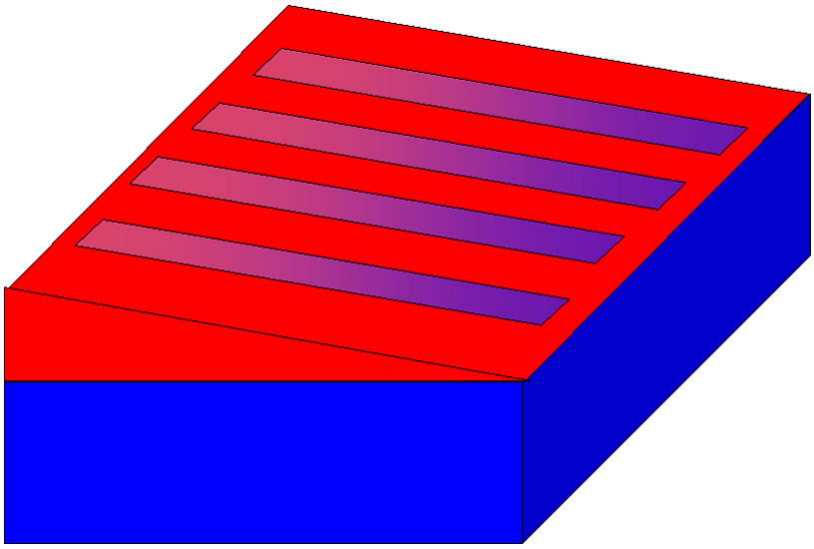

B

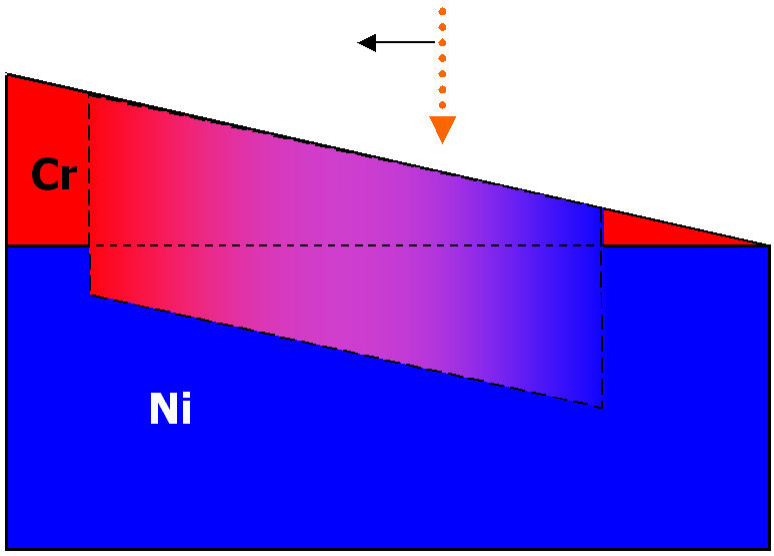

Figure 3: Schematic of a combinatorial sample produced by EBW; A) the e-beam welds run the length of the wedge to create a compositional gradient along the length of the weld; B) cross-section of the sample showing the constant depth of the welds to establish the different compositions.

Material System

While we expect that combinatorial methods will be applicable to a wide variety of materials systems, technique development in this project will focus on the model binary alloy system Ni-Cr, which is a subset of the important Fe-Ni-Cr ternary system. This binary alloy system was chosen for three reasons. First, the Fe-Ni-Cr ternary system forms the basis of many technologically important structural materials including, for example, the H-series and C-series casting alloys used in a wide variety of applications where heat and/or corrosion resistance are required [18]. A partial list of applications in which the H-series alloys are used includes: furnace fixtures; parts for cement/lime kilns and roaster furnaces; coke oven exhausts; gas turbines; and heat treatment fixtures. Clearly, these materials have crosscutting impacts in the chemical processing, heat treatment, metal casting, and steel industries.

Second, since this ternary system has been studied extensively by conventional techniques, its structure, properties, and phase equilibria are readily available for comparison to results obtained by the new combinatorial methods. Producing cast alloy standards for comparison was relatively easy and inexpensive compared to other potential systems.

Third, the Ni-Cr binary system is much easier to produce by vapor deposition than the Fe-Ni and Fe-Cr systems, and its phase behavior is relatively simple. Once developed for this binary alloy system, the techniques could be expanded to the Fe-Cr and Fe-Ni binary systems. It could also be expanded to the Fe-Ni-Cr ternary alloy system by depositing triangular wedges of the two elements onto a substrate of the third element. Alloying of such a specimen could produce a sample that has within it all the individual compositions represented in the ternary Fe-Ni-Cr phase diagram.

As shown in the Ni-Cr phase diagram in Figure 4 [19], nickel and chromium do not exhibit complete solid solubility. Looking at the isotherm at 900ºC, chromium is soluble

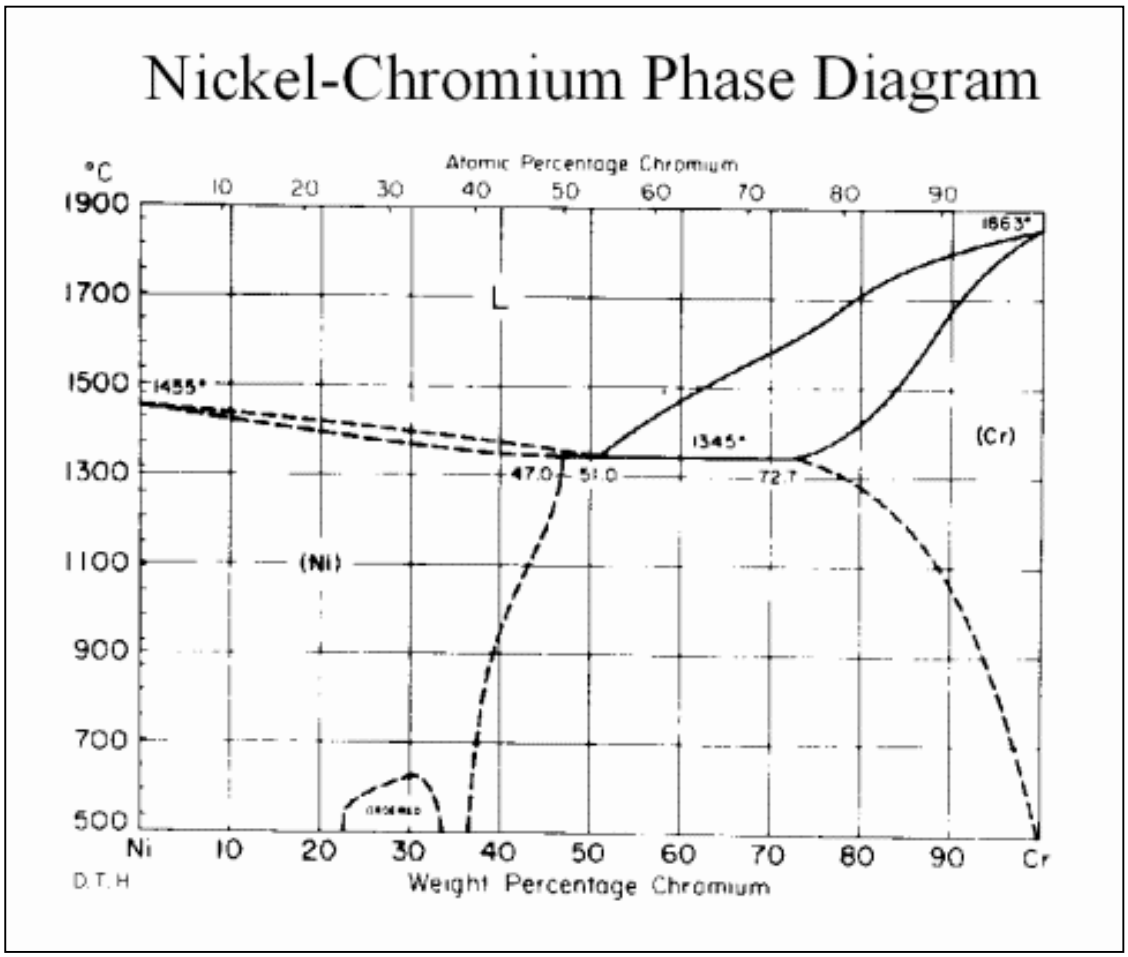

Figure 4: Ni-Cr phase diagram [19].

in nickel up to about 42 at% Cr. This nickel rich phase maintains the face centered cubic (FCC) crystal structure of nickel and is referred as the gamma phase (γ-phase). Nickel is soluble in chromium only between 95 and 100 at% Cr at this same isotherm. This chromium rich phase maintains the body centered cubic (BCC) crystal structure of chromium and is referred to as the alpha phase (α-phase). Between 42 and 95 at% Cr, both the γ-phase and α-phase coexist in a two-phase region, where both phases are saturated solutions [20].

Chapter 2: Procedures

A high-vacuum physical vapor deposition (PVD) system available at ORNL was used to prepare our alloy library specimens. Electron beam heating was used to evaporate high-purity nickel or chromium, and a film was deposited onto a substrate of the other metal. The deposition system was modified to incorporate a moveable shutter placed in the line-of-sight between the targets and the substrate. By translating the shutter parallel to the substrate as the target was vaporized, a wedge shaped film of element "A" was deposited onto substrate "B".

After film deposition, a precision, fully automated EBW system at ORNL was used to alloy the films by local e-beam melting. The beam can melt up to several millimeters deep, and the diameter of the molten zone can be constrained to less than 1 mm, thus minimizing lateral spreading of the alloying components. After alloying of the component species is accomplished, a specimen that is pure "A" at one end and pure "B" at the other is produced, with compositions varying systematically in between corresponding to the entire binary composition range. By controlling the scanning speed and the e-beam power, the heating and cooling rates can be varied, and their effects on film microstructure can be investigated.

Moreover, as shown schematically in Figure 5, several compositional ranges can be produced on the same sample, because the melt depth can be varied up to several millimeters by controlling the e-beam power. This provides an additional degree of freedom in the alloy compositions, since controlling the melt depth can vary the amount of the substrate material incorporated into the alloy. For example, one weld may have a concentration gradient ranging from 0 to 30 at% Cr, while another weld with higher EBW power settings may have a gradient ranging from 20 to 50 at% Cr.

It was initially hoped that one weld of a chromium film on a nickel substrate would establish the full compositional spectrum. However, the compositional ranges along the

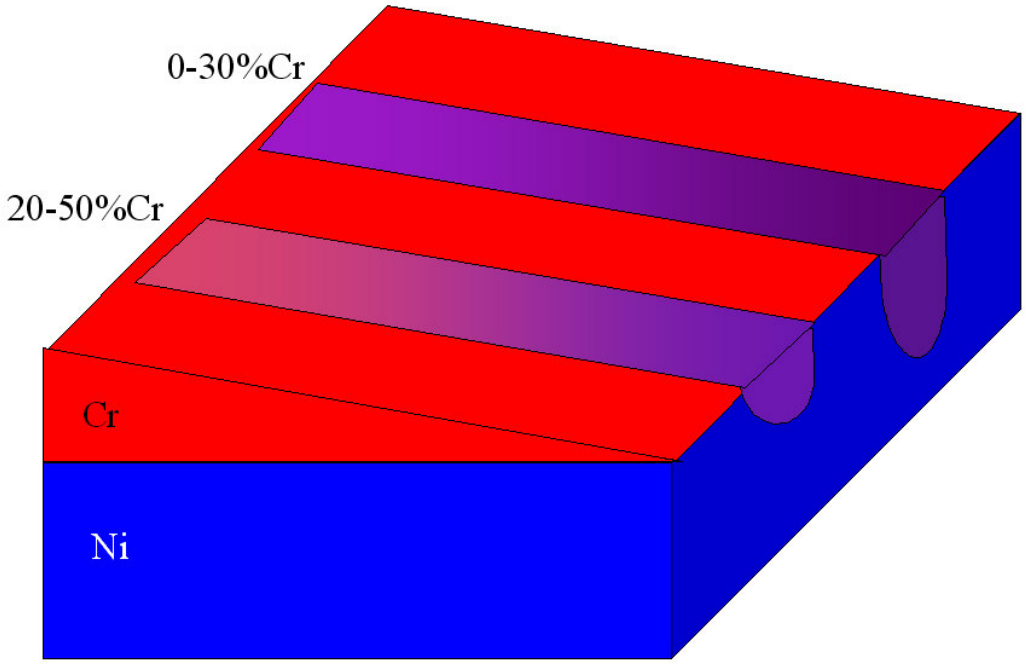

Figure 5: Schematic of a combinatorial sample by EBW showing several compositional ranges.

length of the weld only covered ranges of 30%, and a maximum chromium concentration of 70 at% was achieved. Thicker chromium films were deposited in attempt to overcome this obstacle, but there were limitations related to evaporation, crucible size, and deposition rate measurements. Moreover, when thicker films were deposited, they were unsuccessful due to the films poorly adhering to the substrates. Therefore, EBW of nickel films deposited on chromium substrates was used to achieve the chromium-rich ranges of the alloy system.

Substrate Preparation

To prepare the nickel substrates, a small batch of 99.99% pure nickel was melted and cast into a mold with dimensions of 1" x 0.5" x 6". This cast was warm rolled at 400ºC to a thickness of 0.125" and then cold rolled to 0.060". The finished nickel strip was about 1" wide. The strip was then cut into 1.5" sections and mounted in epoxy with the 1" x 1.5" face down. Likewise, a small batch of 99.99% pure chromium was melted and cast into a similar mold to prepare the chromium substrates. Chromium cannot be rolled, so the casting was cut into 1" x 1.25" sections with a thickness of 0.15". These sections were also mounted in epoxy with the large face down.

The mounts were hand polished to maintain uniform polishing thickness through 600 grit, and then polished using a Struers RotoForce automated polisher with a 6, 3, and 1 μm diamond suspension according to Table 1. The mounted substrates were then soaked methylene chloride overnight to dissolve the epoxy and release the substrates. Ethanol was used to clean the substrates and remove any excess epoxy or methylene chloride. The final thickness of the nickel substrates was approximately 0.058", and the final thickness of the chromium substrates was approximately 0.12".

To ensure cleanliness and avoid contamination, latex gloves were worn each time the substrates were subsequently handled. The substrates were placed polished side up in a beaker of acetone, and the beaker was placed in an ultrasonic bath for five minutes. The

Table 1: Grinding and polishing schedule for Ni-Cr samples.

MATERIAL	Nickel & Chromium Specimens			
GRINDING	PG	FG1	FG2	FG3
BASE	PIANO	PIANO	PIANO	PIANO
ABRASIVE	DIAMOND	DIAMOND	DIAMOND	DIAMOND
GRAIN SIZE	#120	#220	#600	#1200
ROTATION	→	→	→	→
LUBRICANT	WATER	WATER	WATER	WATER
SPEED RPM	300	300	300	300
FORCE	30N	30N	30N	30N
MINUTES	UNTIL PLANE	1:30 MIN	2:30 MIN	2:30 MIN
POLISHING	DP	DP1	DP2	DP3
CLOTH	ALLEGRO	LARGO	DP-DAC	DP-NAP
ABRASIVE	DIAMOND	DIAMOND	DIAMOND	DIAMOND
GRAIN SIZE	6 MICRON	6 MICRON	3 MICRON	1 MICRON
ROTATION	→	→	→	→
LUBRICANT	DP - LUB	DP - LUB	DP - LUB	DP - LUB
SPEED RPM	150	150	150	150
FORCE	30N	30N	30N	30N
MINUTES	8:00 MINS	8:00 MINS	8:00 MINS	5:00 MINS
COMMENTS:	GRINDING TIMES MAY VARY DUE TO THICKNESS OF MATERIAL			

substrates were then rinsed with deionized water. The substrates were placed polished side up in a beaker of ethanol, and the beaker was placed in an ultrasonic bath for five minutes. The substrates were again rinsed with deionized water. Compressed air was used to dry the substrates. Sample holders were used to carry and protect the substrates while being transported between labs.

Physical Vapor Deposition

A CVC physical vapor deposition (PVD) chamber was used to deposit films (see Figures 6 and 7). This system used a Telemark-271 electron beam gun to heat the source material for vaporization. The samples were inverted directly above the source material and were attached to a mounting stage. A moveable shutter directly below the mounting stage moved continuously during deposition to create a wedged film on the substrate.

The mounting stage was removed from the chamber and set upside down on a table before the substrates were mounted. The substrates were mounted onto the mounting stage with screws, where the heads of the screws held the substrates to the stage. Only two or three screws were required, enabling the substrates to be held with minimal surface covered. The mounting stage was reinstalled into the PVD chamber with the mounting bolts. The stage was then rotated so that the desired wedge direction was parallel to the travel direction of the shutter. Clearance between the substrate holding screws had to be checked to ensure that the shutter could freely move without hitting the tops of the screws. If there was insufficient clearance, washers were added under the mounting stage in line of the mounting bolts. The wires were connected from the computer to the shutter motor and the stage rotating motor.

The source crucibles were filled with pure metal of the intended film metal. If a chromium film was to be deposited on a nickel substrate, then pure chromium pellets were added to the source crucible. However, if a nickel film was to be deposited on a chromium substrate, then it was best to use a cast nickel button at the bottom of the

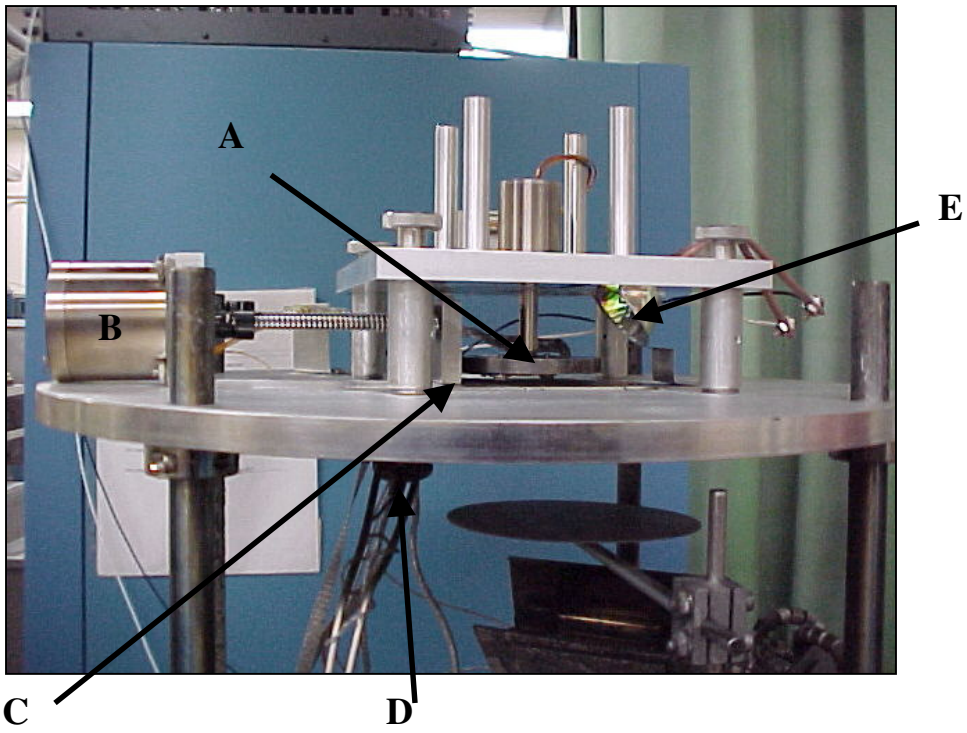

Figure 6: Inside of the PVD chamber; A) sample holder; B) motor that drives the shutter to create the wedged film; C) moveable shutter; D) quartz microbalance; and E) heater lamp.

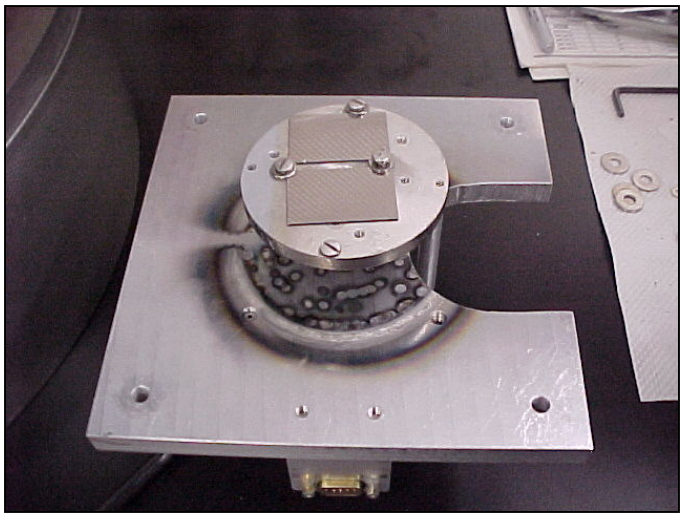

Figure 7: Sample holder with two Ni substrates attached to it.

source crucible. A new quartz crystal microbalance was inserted so that the deposition rate and the film thickness could be measured. The computer that controls the crystal microbalance was checked to ensure that the crystal could be recognized. If the computer didn't properly identify the microbalance, the microbalance was removed and reinstalled. Vacuum grease was added to the chamber seal gasket if needed, and then the chamber was closed. Both the roughing pump and the turbo pump were turned on, and the system was left over night to establish the best vacuum.

After the chamber had reached a vacuum of less than 1.0×10^{-7} Torr, the heater lamp near the stage was turned on and the lamp power was increased to 20 volts and 6 amps. The samples were heated for about 90 minutes to raise the temperature of the substrates to approximately 90ºC. This higher temperature aided in the adhesion of the metal vapor to the substrates. The appropriate density and z-ratio (acoustic impedance ratio) of the source metal was programmed into the computer controlling the crystal microbalance to provide accurate measurements. The density and z-ratio of nickel are 8.91 g/cm^3 and 0.331, and the density and z-ratio of chromium are 7.20 g/cm^3 and 0.305, respectively.

The computer that controlled the moveable shutter was turned on, and set so that the shutter used the "wedge" program, with the sample size of 1.5", shutter time of 120 seconds, and open dwell time of 0 seconds. The power settings to the e-beam source were turned on and allowed to warm up a few minutes before proceeding. The accelerating potential and current controls were turned on, and the accelerating potential was slowly increased to 10 kV at a rate of 1 kV every 10 seconds. The current was increased slowly until the crystal microbalance began to detect some deposition. This usually happened around 30 mA for chromium and 80 mA for nickel. The beam position and amplitude was adjusted to optimize the deposition rate, while trying to maintain a rate of 12-16 Å/sec for chromium and a rate of 3-6 Å/sec for nickel. The "begin cycle" button was pushed on the computer that controlled the shutter, and the "start" button was pushed on the computer that monitored the crystal microbalance.

Chromium has a faster deposition rate than nickel due to its higher vapor pressure. The deposition rate of chromium could be increased beyond 16 Å/sec, but it was kept lower to increase adherence to the substrate and to establish a uniform wedged film. For chromium films, it was best to use a lower amplitude setting and move the e-beam often to maintain a uniform deposition rate. Due to its high vapor pressure, the chromium would sublime into a vapor state without melting first. For nickel films, it was best to use a higher amplitude setting that covered the majority of the cast nickel button. High current was needed to first melt a large pool on the button, allowing a large area of molten nickel to then vaporize.

When the desired thickness was achieved by observing the measurements from the quartz microbalance, the "end cycle" button was pushed on the computer that controlled the shutter. When the shutter was closed fully, the computer indicated that the cycle was over. Then the e-beam current was reduced to zero, and then the accelerating potential was slowly reduced to zero. Both the current and the accelerating potential were turned off, and then the main power to the system was also turned off. The heater lamp next to the stage was then turned off, and the system was left over night to allow the chamber to cool before opening. The next morning the chamber was vented and the samples were removed. The samples were placed in sample holders until they could be e-beam melted.

Electron Beam Melting

A Leybold-Heraeus electron beam welder was used to create the welds that alloyed the nickel with the chromium. The samples were loaded such that the direction of the wedge ran parallel to the x-direction of the welder. This simplified the later process of programming the welding direction. The samples were clamped down well to ensure that any vibrations caused within the welder would not move the samples. This also helped to prevent a wavy weld line.

The welder could not be used until the vacuum had reached a pressure of less than $3.2x10^{-4}$ Torr. The accelerating potential, current, and travel speed were adjusted, and the welder was positioned near the sample at one end of the film's wedge (most often the side with the small end of the wedge). The computer was programmed to specify the direction and travel distance of the weld.

The welder started about 1cm from the edge of the sample, then traveled at a constant speed over the sample in parallel to the direction of the wedged film. The welder did not stop until it was about 1cm off the edge of the sample. This helped to create a weld of uniform size and depth. A table of successful weld parameters used for the samples is shown in Table 2.

Ni-Cr Alloy Standards

Standards of pure nickel and chromium were arc melted in a water-chilled copper mold, as were seven Ni-Cr alloys with chromium concentrations of 20, 30, 40, 50, 56.14, 70, and 85 at%. The chromium and nickel starting materials were greater than 99.995% purity. The pure metals were carefully weighed and then mixed by arc melting, with the buttons flipped and re-melted five times to ensure good mixing. Total weight losses after melting and casting were less than 0.2%, which led to negligible changes in alloy composition after melting. All chromium concentrations of samples and cast standards are measured as atomic percent (at%).

The standards were cross-sectioned, mounted in epoxy, and polished through a 1 μm diamond suspension according to Table 1. The standards were examined by optical microscopy, SEM, EDS, and nanoindentation, and this data was used as a comparison for all of the welded combinatorial samples.

Table 2: EBW parameters for Ni-Cr samples.

	Sample	Weld	Voltage (kV)	Current (mA)	Speed (ipm)
Cr film on Ni substrate	EB2 no wedge	2	150	1.0	50
		3	150	0.9	50
		4	150	0.8	50
		5	150	0.7	50
	EB3	1	100	1.1	20
	EB6	2	100	1.1	10
		5	120	0.9	10
		8	130	0.8	10
	EB7	2	100	1.1	20
		4	150	1.0	50
		5	150	0.9	50
		6	150	0.8	50
	EB8	2	100	1.1	10
		4	120	0.9	10
		7	130	0.8	10
		8	130	0.9	10
Ni film on Cr substrate	EB9	4	120	0.9	10
		5	120	1.0	10
		6	120	1.1	10
		7	120	1.2	10
		8	120	1.3	10
	EB10	5	100	1.3	10
		6	100	1.4	10
		7	100	1.5	10
		8	100	1.6	10

Specimen Characterization

The scientific challenge with respect to specimen characterization is to develop sensitive probing techniques that can be applied rapidly at small scales. A few techniques were already available that could be relatively easily adapted with adequate spatial resolution to the characterization of the combinatorial alloy libraries. The focus was on these techniques to demonstrate proof-of-principle as described below.

Though not capable of determining crystal structure and orientation, the scanning electron microscope (SEM) was used to visually identify phases within the welded sample. The backscattered electron (BSE) detector was used to enhance the contrast between the phases of the binary system. The magnification capabilities of the SEM also enabled visualization of grain boundaries, voids, microsegregation, and the interaction between the deposited film and the weld pool.

The elemental compositions were determined by EDS, which works in conjunction with the SEM. The EDS detects secondary electrons from a region as small as 1 μm by 1μm, and a maximum detection depth of about 1 μm. This provided composition details for the small regions of secondary phases, as well as covering large regions such as the weld surface. The EDS is computer interfaced, and uses a software package called Revolution. This software provides a quantitative measurement showing the composition of each element within the combinatorial array with a standard deviation of less than 3% [21].

In conjunction with the above chemical and structural characterizations, nanoindentation was used to investigate the fundamental mechanical properties of the combinatorial specimens. The goal was to correlate mechanical properties with chemical composition and microstructure. There is a great deal of experience in this area, and several fully automated, state-of-the-art nanoindentation systems were available for use. The two mechanical properties that can be most easily probed are elastic modulus and hardness [22], both of which can be measured with spatial resolutions greater than 1 μm.

The nanoindenters were set up to make a series of indentations at specified locations on the alloy library surface and automatically collect and store all the data needed to obtain hardness and modulus as a function of position on the combinatorial sample surface. Approximately 50 to 100 indentations could be made during an overnight run, depending upon the set-up parameters. Thus mechanical properties could be obtained over a fairly wide range of chemical composition in a relatively short time.

The quality of the specimens was assessed by preparing a select set of Ni-Cr binary alloys by conventional melting and casting and comparing their mechanical properties measured by nanoindentation with those of the combinatorial specimens.

Metallography

Samples for cross-sectional examination were cut with a slow-speed diamond saw to ensure that the film did not peel off of the substrate. Before cutting, the samples were wrapped with a paper towel to prevent scratches on their surface. The arc melted standard alloys were cut with electrical discharge machining (EDM). Additional grinding was necessary to pass through the heat affected region caused by the EDM. The samples were set in epoxy mounts for examination.

The metallographical procedures were performed using Struers polishing equipment, which included a RotoForce-4 polishing arm, Lupo lubricant drip regulator, and a Rotopol-25 polishing wheel. The final polishing stages used Wendt Dunningham diamond suspensions of 6, 3, and 1 μm. Polishing procedures followed those outlined in Table 1. Sometimes the samples were placed on a vibrating silica bowl with 0.5 μm silica for several hours to produce a better finish.

SEM and EDS

Samples that were evaluated from the surface often did not need carbon coating, but there were several instances when a coating was necessary to enhance the imaging and detection capabilities. All cross sections required carbon coating due to the nonconductive nature of the epoxy mounts.

A Hitachi S4100 SEM at the High Temperature Materials Laboratory (HTML) at ORNL was used. To produce high quality images, lower voltages were often used to minimize charging. Most commonly the accelerating voltage was 5-10 kV, the condenser lens was set at 11, and the stage distance was 15 mm. A Gresham Sirius detector system was used for the EDS measurements. To excite all chromium and nickel peaks, the accelerating voltage was increased to 20 kV, the condenser lens was reduced to 9, and the stage distance was increased to 20 mm.

The analysis software for the EDS system was Revolution from 4pi Analysis, Inc. Revolution uses ZAF corrections based on the relation:

$$\frac{C}{C_{sd}} = \frac{I}{I_{sd}} \frac{F}{F_{sd}}$$

where **C** is concentration, **I** is x-ray line intensity, and **F** is the ZAF matrix correction. The subscript **SD** refers to the same quantities for the standard element in use for the analysis. If standardless analysis is used, a mathematical model for the standard is substituted [21].

The EDS system and analysis software were tested using a Ni-70Cr alloy standard to determine their accuracy. A large section of the alloy was selected, because a point measurement could isolate on a single phase in the two-phase alloy. The standard alloy was measured three times, and each measurement was within 0.5% of the expected value. Figure 8 shows an EDS spectrum of the Ni-70Cr alloy standard with the measured quantitative composition values.

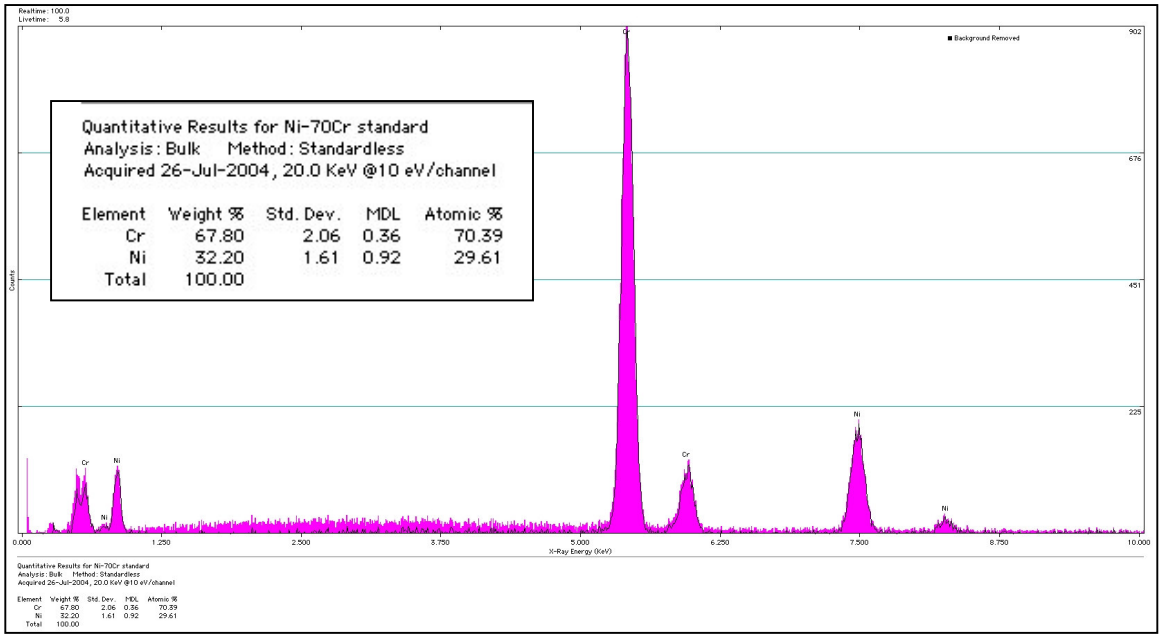

Figure 8: EDS spectrum and quantitative measurement of Ni-70Cr cast standard.

Nanoindentation

A NanoII nanoindenter from MTS with a Berkovich indenter was used for mechanical property measurements. The continuous stiffness mode was used with the frequency set to 45 Hz. The surface search distance was 9000 nm, and the maximum drift rate prior to tests was 0.1 nm/sec. The loading rate was 0.05 nm/sec and the unloading rate was 300 nm/sec. Indents were made to a maximum depth of 1000-1200 nm for weld surface tests, and to a maximum depth of 400-600 nm for weld cross-section tests. Indents were made to a maximum depth of 200-400 nm for all polished cast standards.

As shown in Figure 9, surface indents were positioned down the centerline in an array from one end of the weld to the other with indent spacing around 800-1000 nm. Most positions were set-up in an array, although some indents had to be individually positioned to avoid the surface cracks, especially in the welds at higher chromium concentration. Indents on the cross sections of the weld were individually positioned to ensure that they were within the alloyed region. Figure 10 shows an SEM image of a typical indent made in the weld surface.

Poisson ratios of 0.31 and 0.21 were used for the nickel and chromium standards, respectively. A Poisson ratio of 0.25 was used for all other alloy standards, and for all welded samples. Results were obtained from data taken at depths of 800 nm for all indents taken from the weld surface and of 400 nm for all indents taken from the weld cross sections. Results of the cast standards were measured from the data taken at a depth of 200 nm.

The accuracy of the NanoII modulus data is usually expected to be within 10% of the literature values. The data for the combinatorial EB welds was compared with the data from the cast standards to validate the precision of the EB weld hardness and modulus.

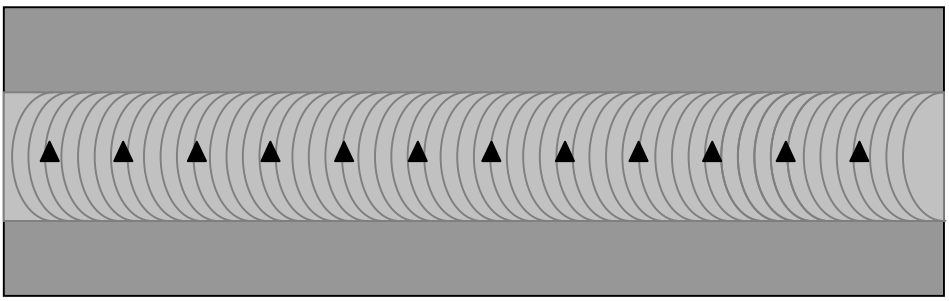

Figure 9: Schematic showing nanoindentation indent positions along the length of the EB weld.

Figure 10: SEM image of typical indent made in the EB weld surface.

Chapter 3: Results and Discussion

Results will be discussed for Ni-Cr standards, samples made with chromium films on nickel substrates, and samples made with nickel films on chromium substrates. The results from the welded samples are compared with the results from the alloy standards to determine if the combinatorial welds will have similar properties to those of cast structures.

Cast Ni-Cr Standards

Cross sections of the Ni-Cr cast standards were made to examine the microstructure at different compositions. Two-phase microstructures were not observed in the cast standards of 20, 30, or 40 at% Cr, but were seen in the standards of higher chromium concentrations. Figures 11 shows a micrograph of the Ni-30Cr cast standard, which shows evidence of microsegregation within the solid solution. Figure 12 shows a micrograph of the Ni-70Cr cast standard. The light regions are the chromium rich α-phase, and the dark regions are the nickel rich γ-phase. The casting shows a dendritic structure, with the dendritic direction toward the center of the cast button, as expected. There was more cracking and voids in the standards as the chromium concentration increased due to the large solidification temperature range.

The standards were tested by nanoindentation to evaluate the mechanical properties of hardness and modulus. The surfaces were polished through 1 μm diamond suspension prior to testing. The polishing reduced the data scatter and yielded results with low deviation. For the standards with one phase, indents were made in a regular 3x4 pattern to obtain enough data to determine uniformity. For the standards within the binary phase region, several indents were made individually on the γ-phases and the α-phases, and indents were also made in a regular 3x4 pattern to examine both phases and regions near phase boundaries. More indents were made in the Ni-70Cr cast standards to ensure that both phases were sampled to obtain the full hardness spectrum of the phases.

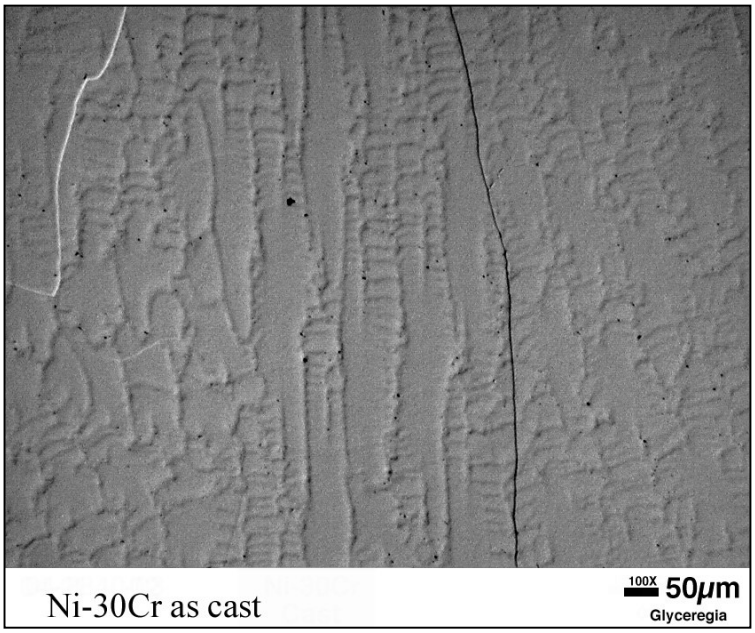

Figure 11: Optical image of the Ni-30Cr cast standard at 100x magnification.

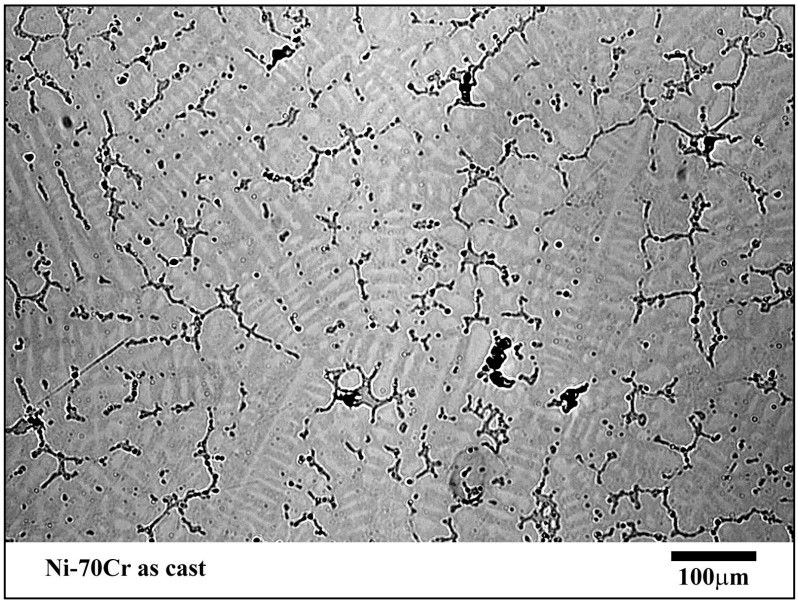

Figure 12: Optical image of the Ni-70Cr cast standard at 100x magnification.

According to the Ni-Cr phase diagram in Figure 4, there are three regions of interest: the nickel rich solid solution (γ-phase), the chromium rich solid solution (α-phase), and a dual phase region. The elastic modulus of alloys is strongly dependent upon elemental composition, and other characteristics such as phases, heat-treatments, or surface conditions exert a negligible influence [20]. For the sake of discussion, it is useful to compare the measured moduli to those predicted by a simple linear rule of mixing. In this case, the modulus should show a linear tendency between the modulus of pure nickel (200 GPa) and the modulus of pure chromium (279 GPa) [20].

Hardness on the other hand, is dependent on many factors besides just alloy composition. Phase distribution, grain size, and surface conditions can have a great effect on the measured hardness of the alloy. Therefore, a linear "law of mixing" is not necessarily useful, except in single-phase regions where solid solution strengthening may be important.

Figure 13 shows the nanoindentation elastic modulus results for the Ni-Cr alloy standards. The modulus of the pure nickel standard averaged 194.7 GPa, and the modulus of the pure chromium standard averaged 277.1 GPa, both of which are very similar to the literature values of 200 and 279 GPa, respectively. The "law of mixing" line shown in the figure represents the linear expectancy of the modulus between 200 and 279 GPa.

The data points for the Ni-Cr cast alloys were all within the general tendency of the "law of mixing", though there were several points for the higher chromium alloys that were higher than expected. The standards up to 40 at% Cr all had data points within 10% of the "law of mixing" line, but the standards of 50 and 56.14 at% Cr had several modulus measurements that fell as much as 17% below the "law of mixing" line. The cast standards of 70 and 85 at% Cr were on the other end of the spectrum, with some of the modulus measurements reaching more than 30% higher than the "law of mixing" line.

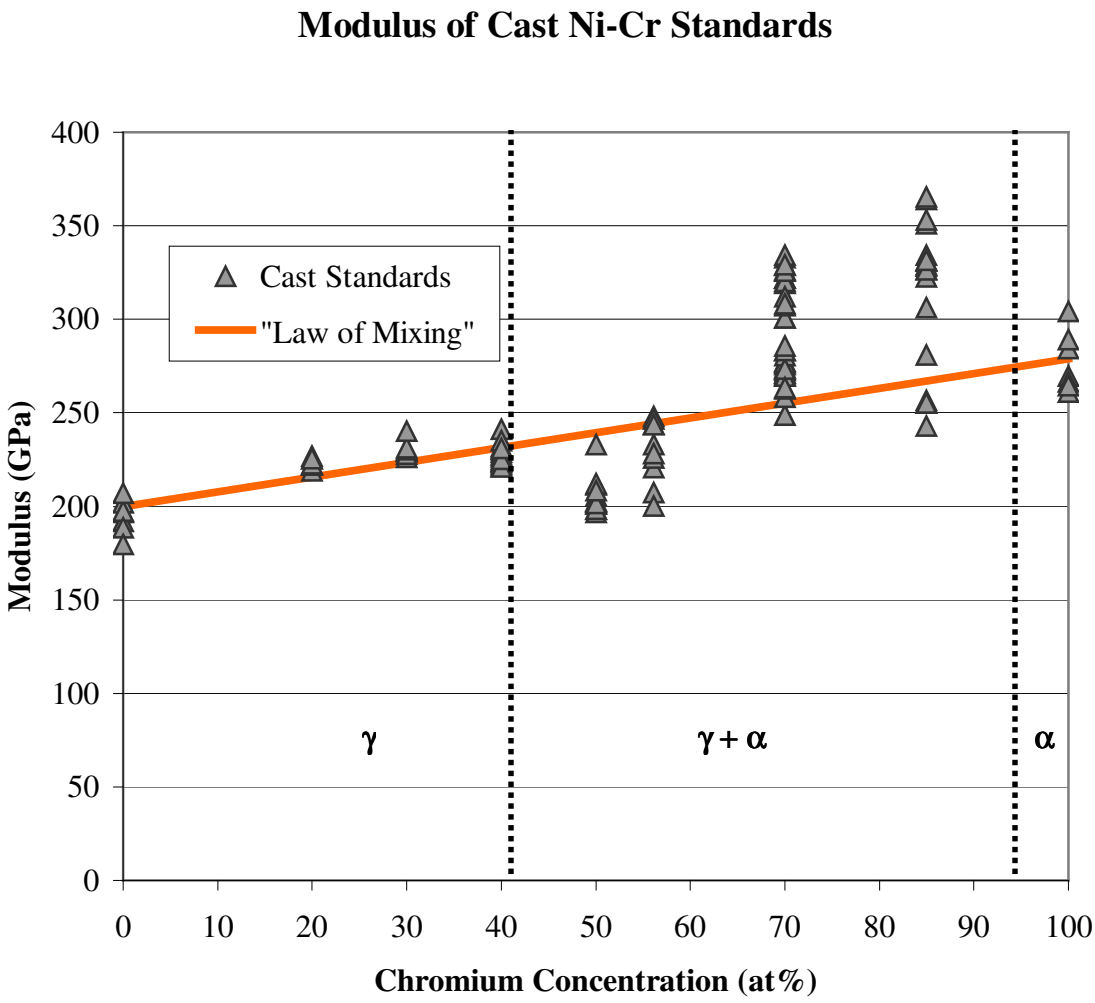

Figure 13: Modulus of cast Ni-Cr standards.

Although the modulus should be primarily dependent only on the total composition, it should be noted that the indents were so small that they often hit parts of or all of only one phase within the alloy. This explains the scatter in the two-phase regions. Assuming the 900ºC isotherm of the Ni-Cr phase diagram, the saturated γ-phase should have a chromium concentration near 40 at%, and the saturated α-phase should have a chromium concentration near 95 at%. This would cause the individual phases to have moduli varying between approximately 232 and 275 GPa, respectively. The actual scatter in the data is somewhat greater.

The hardness values for the cast Ni-Cr alloy standards are shown in Figure 14. The hardness values up to 40 at% Cr show very little deviation and an upward tendency with a generally constant slope. This is consistent with the expectations of the single-phase region as it reaches its solid solution solubility limit. The hardness of pure nickel was about 1.2 GPa, and the hardness of the Ni-40Cr alloy was about 3.1 GPa. There were no dual phases observed in the cast alloys less than 40 at% Cr. At 50 at% Cr, the hardness data begins to increase at a much steeper slope and the scatter becomes greater. The hardness values of the Ni-70Cr and Ni-85Cr standards extend from 7 and 8 GPa to nearly 13 GPa.

Figure 15 shows an image of thirty indents made in a 6x5 pattern spaced 6 μm apart in the Ni-70Cr cast standard. The indents resided in both the γ-phase and the α-phase, and make a clear distinction between the hardness of the two phases. Figure 16 shows a contour plot of the hardness values resulting from these indents. The measurements from the indents that struck clearly in only one phase were used to estimate the hardness of the two phases, and it was found that the hardness of the γ-phase was 4.25 GPa and the hardness of the α-phase was 11.57 GPa.

The hardness of the γ-phase at the solubility limit is in the range of 3-4 GPa. However, alloys with greater than 54 at% Cr will have α-phase regions and γ/α eutectic regions. Therefore it is difficult to isolate the γ-phase for nanoindentation because it is finely

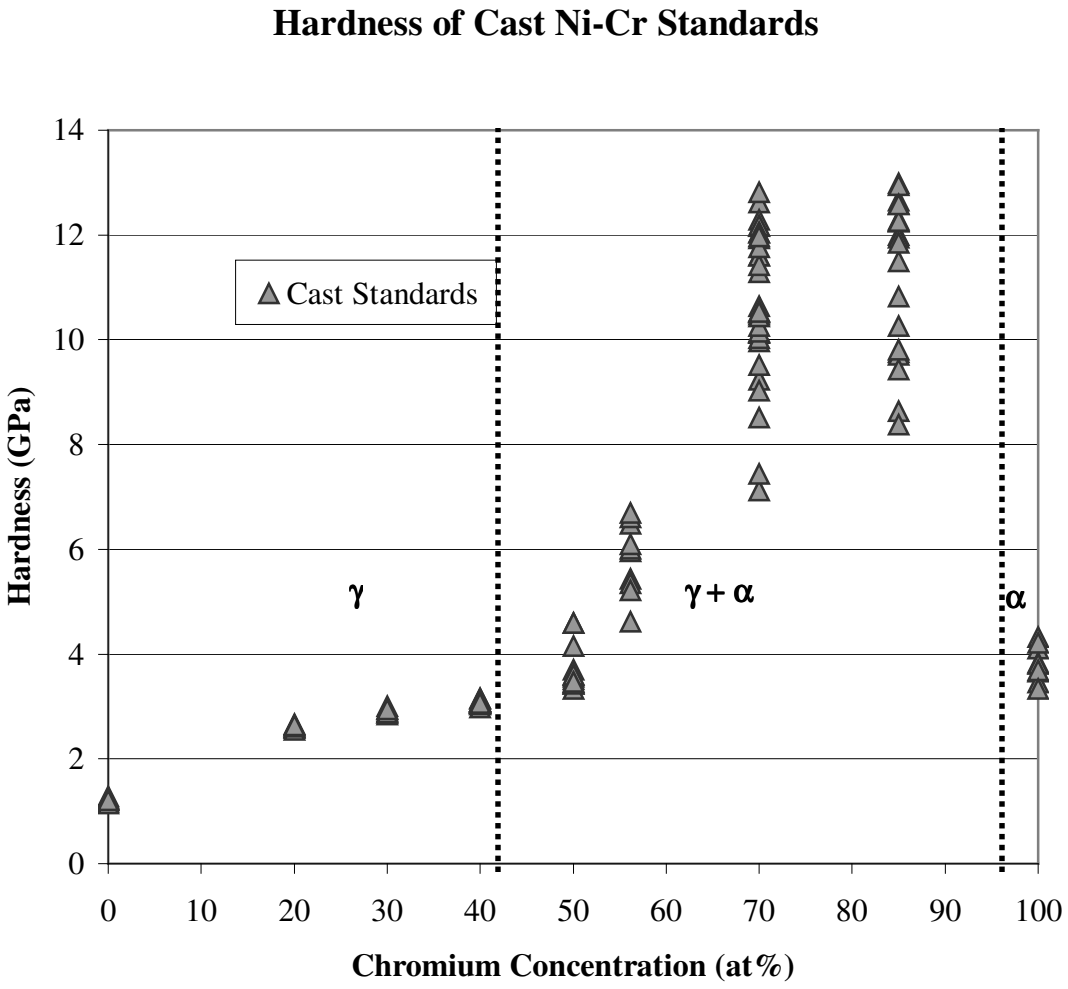

Figure 14: Hardness of cast Ni-Cr standards.

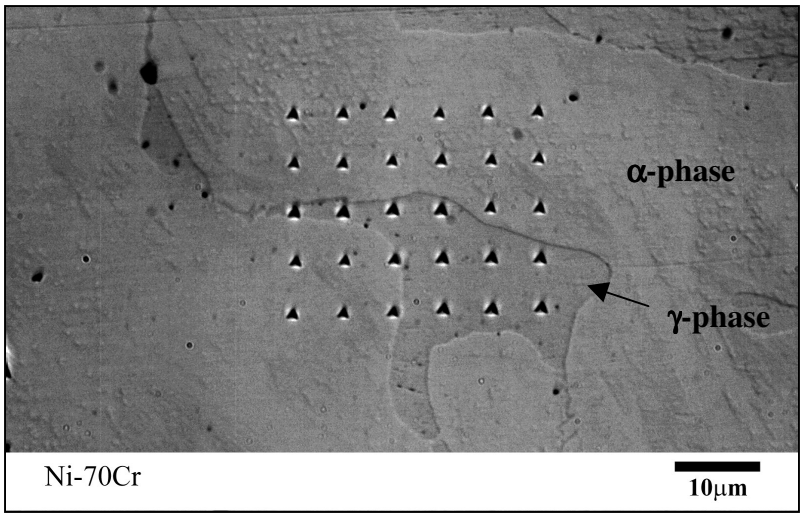

Figure 15: Optical image of an indent pattern covering both phases within the Ni-70Cr cast standard.

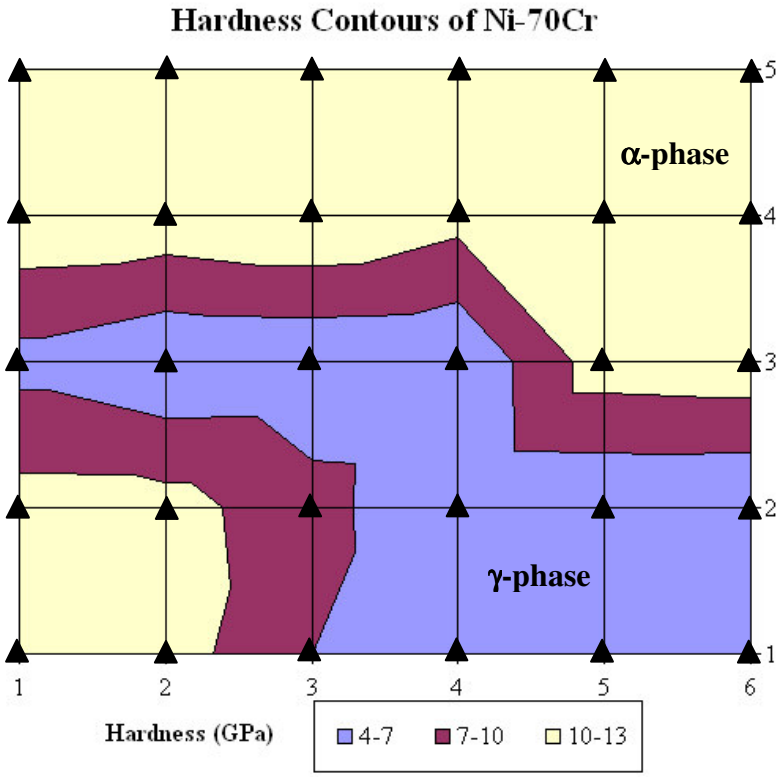

Figure 16: Hardness contour plot of indent pattern covering both phases within the Ni-70Cr cast standard.

intermixed in a eutectic. This eutectic can be seen in the Ni-85Cr standard shown in Figure 17, where the light regions are the nickel rich γ-phase and the dark regions are the chromium rich α-phase.

The large deviation is primarily due to the binary phase region that occurs above 50 at% Cr, although it was also observed that the alloys with higher chromium concentration had a higher tendency for cracks and voids. These cracks and voids were also visible in the cast pure chromium, which explains why the scatter of hardness for chromium was so much higher than for nickel. The hardness of pure chromium was about 3.8 GPa.

The hardness values obtained by nanoindentation were verified by Vickers microhardness as well. Figure 18 shows the hardness results obtained from the VH200 microhardness tests using a load of 200 g. The same tendencies are shown by microhardness as by nanoindentation. The absolute hardness values cannot be directly compared due to differences in the definitions of Vickers and Berkovich hardness, as well as differences in loads used to make the measurements.

Chromium Films on Nickel Substrates

The chromium films adhered well to the nickel substrates, and alloy libraries were made very easily compared to the samples of nickel films on chromium substrates. Figure 19 shows an example of the welded samples with wedged chromium films on nickel substrates. The sample had to be cut in half due to the size limitations of the SEM and nanoindenter.

Figure 20 shows some typical top views of the EB welds. The picture on the left shows the weld at the thin end of the chromium film wedge, and the picture on the right shows the weld at the thick end of the chromium film wedge. It was apparent that the welds had a much rougher surface on the end of the sample with the thicker chromium film.

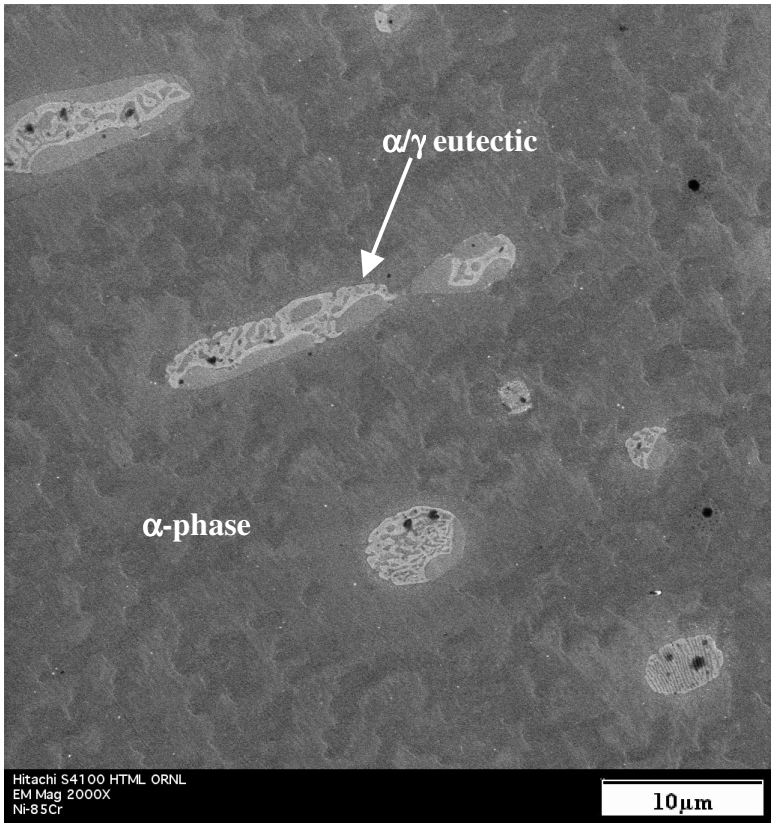

Figure 17: SEM image of the cast Ni-85Cr standard showing eutectic regions at 1000x magnification.

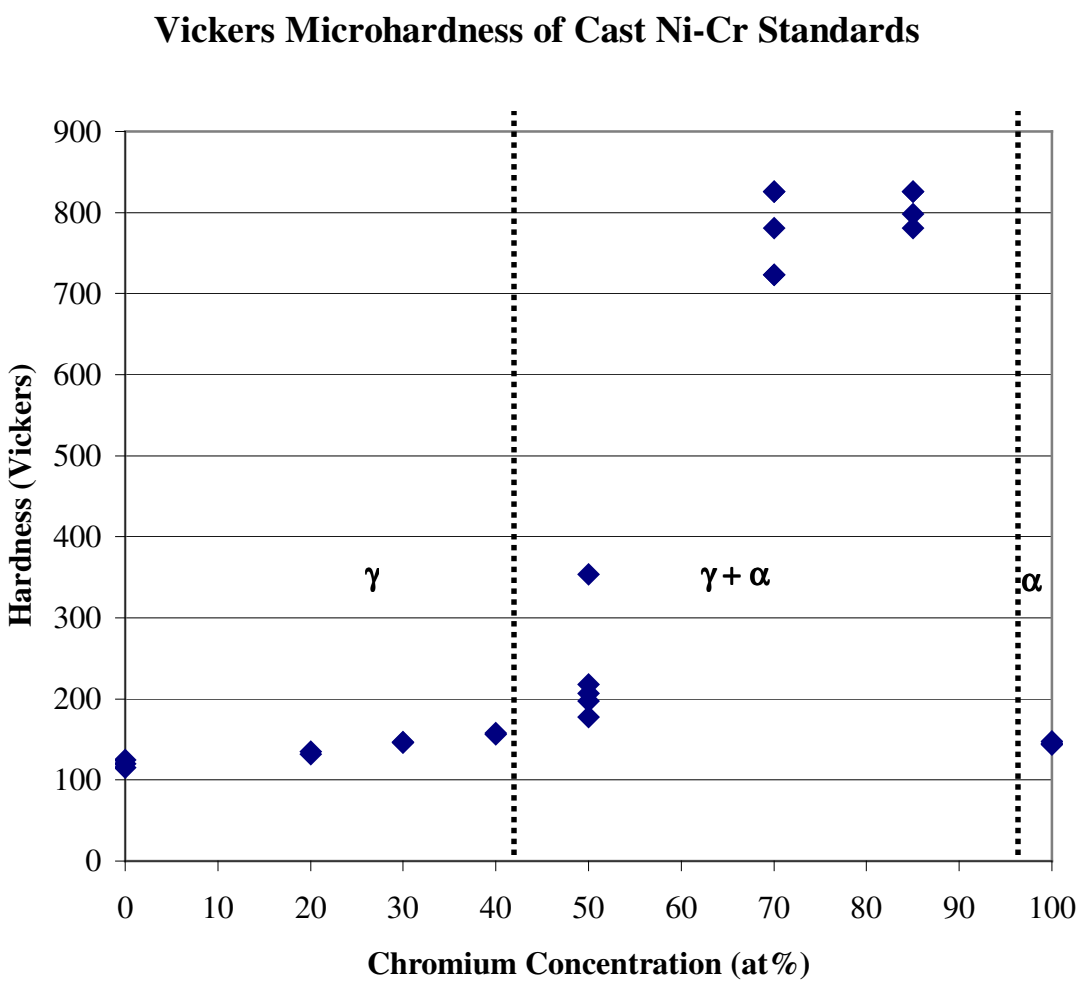

Figure 18: Vickers microhardness of cast Ni-Cr standards.

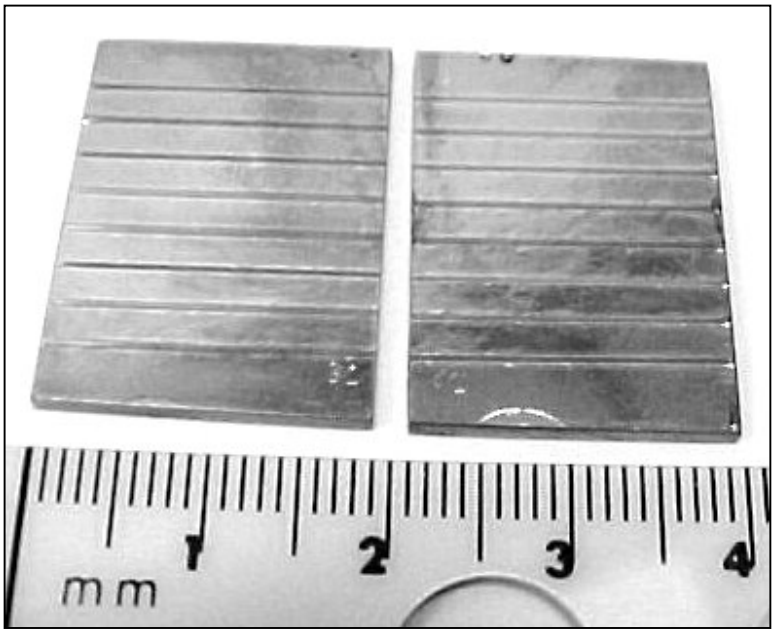

Figure 19: A finished Ni substrate sample with eight combinatorial EB welds across the length of the wedged Cr film.

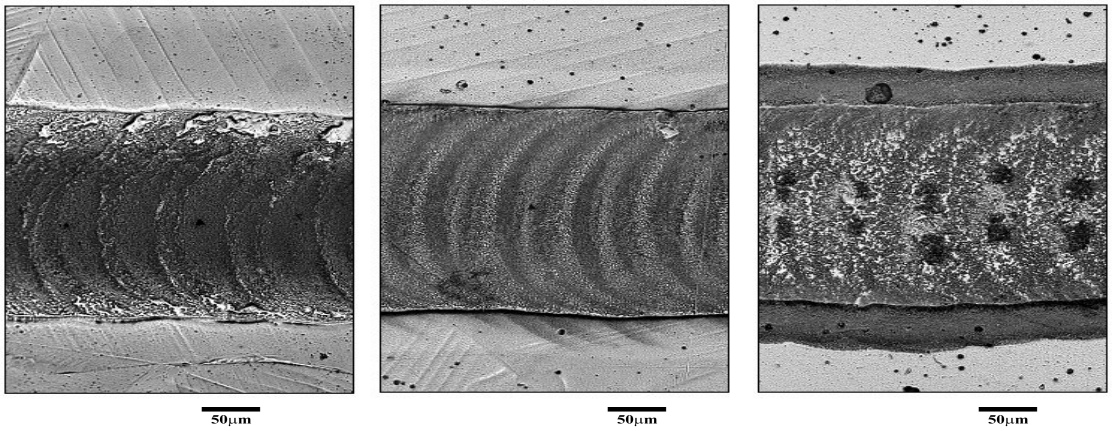

Figure 20: Optical micrographs of typical of EB weld surfaces for Cr films on Ni substrates.

Several EBW parameters were found to greatly affect the characteristics of the weld. As expected, increases in current and accelerating potential increased the depth of the weld, with the accelerating potential having the greatest affect. The travel speed of the weld played a factor in the surface characteristics of the weld, which can have a great affect on the nanoindentation results. Figure 21 compares a weld made at a travel speed of 50 ipm with a weld made at 10 ipm. The weld with the faster travel speed has a wave-like appearance with non-uniform edges, and the surface appears very rough. The weld with the slower travel speed appears much smoother and more uniform. Higher accelerating potentials also caused the welds to be rougher.

The EBW accelerating potentials that created a suitable weld were between 100 kV and 130 kV, although several welds were also created at potentials of 150 kV with faster travel speeds. The current depended on the potential used; the best welds were created when the power (current x potential) was near 100 W. The better welds used a travel speed of 10 ipm.

Figure 22 shows a backscattered electron (BSE) image of a cross-section taken at the thick end of the film. The EBW parameters were 130 kV, 0.8 mA, and 10 ipm. The chromium film can be seen on both sides of the weld, and the weld pool can be distinguished from the nickel substrate. Chromium has a much higher melting point than nickel (1875ºC and 1453ºC, respectively), which can explain why the weld pool begins slightly under the still intact chromium film. At the surface of the weld pool near the edges are darker regions within the lighter weld pool. These darker regions are either unmelted pieces of the chromium film or regions of α-phase, but there was not enough evidence to reach a definitive conclusion. The surface of this weld was examined by EDS and determined to have a chromium concentration of 44 at%, which is around the concentration where the α-phase may form in the γ-phase matrix.

Figures 23 and 24 show more cross-sectional images taken with an optical microscope after the samples were etched with glyceregia to reveal the microstructure. The EBW

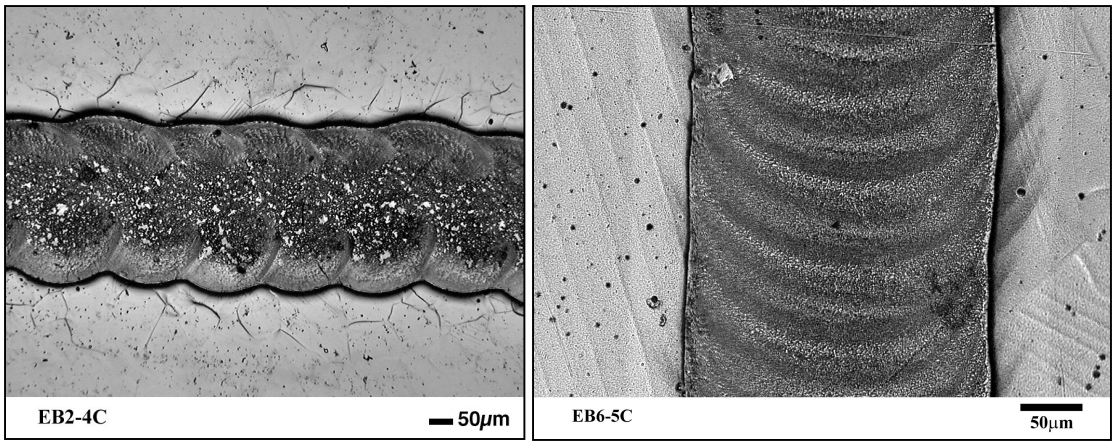

A B

Figure 21: Optical micrographs of weld surface comparing weld speeds of A) 50 ipm, and B) 10 ipm.

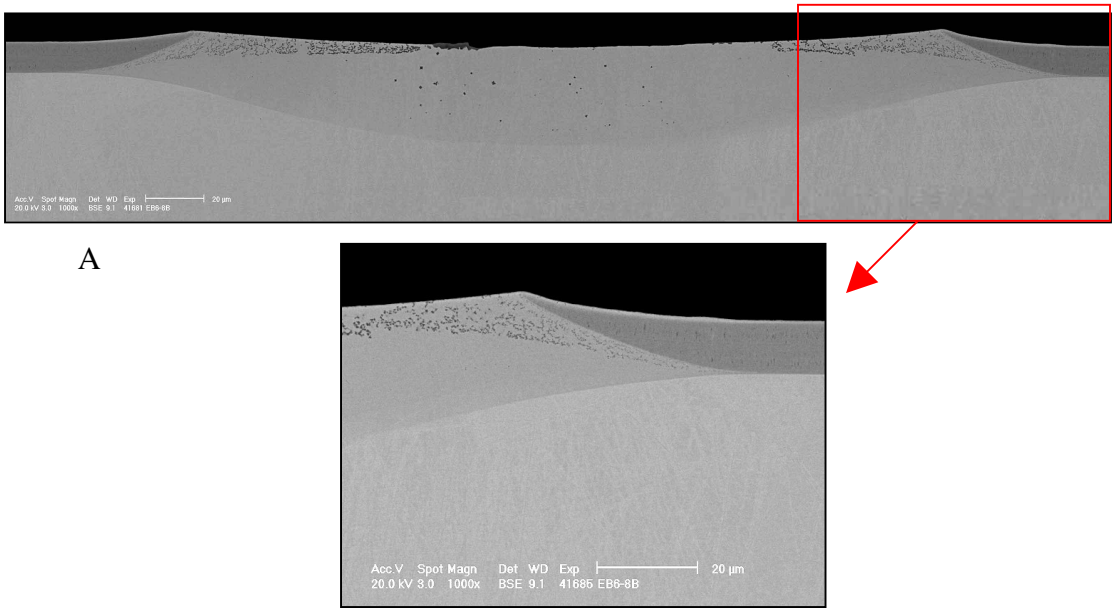

A

B

Figure 22: BSE images of a weld cross section; A) full weld pool, and B) edge of same weld at higher resolution (concentration of about 44 at% Cr).

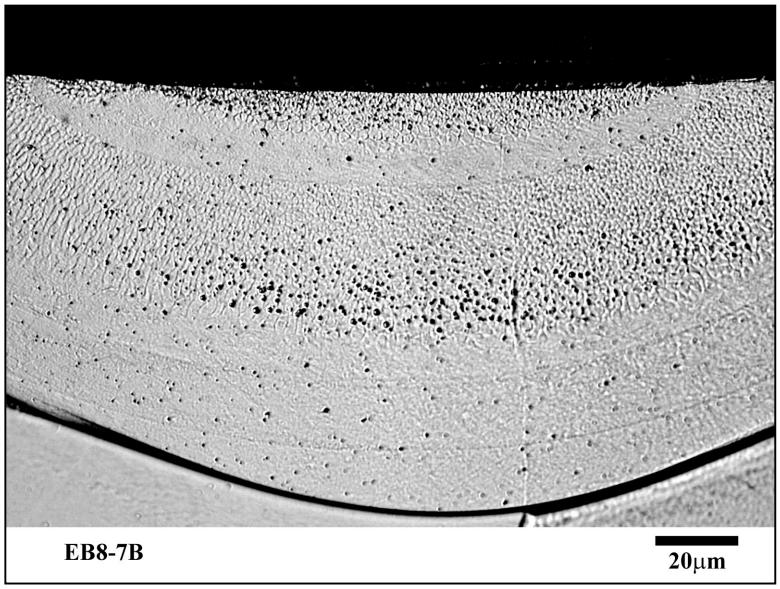

Figure 23: Cross section of EB weld (130kV, 0.8 mA, 10 ipm) at 500x magnification (concentration of about 22 at% Cr).

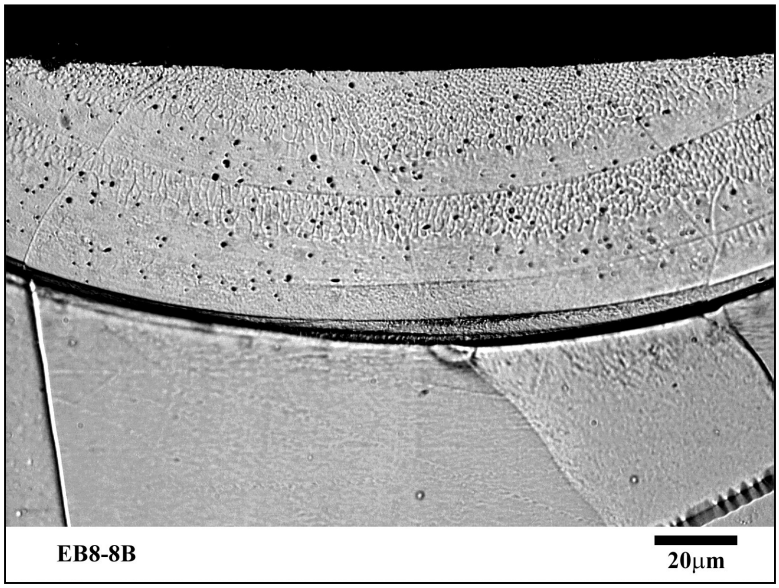

Figure 24: Cross section of EB weld (130kV, 0.7 mA, 10 ipm) at 500x magnification (concentration of about 10 at% Cr).

parameters were a potential of 130 kV, current of 0.7 and 0.8 mA, and travel speed of 10 ipm. Several lines can be seen in the welds that were caused by the movement of the electron beam. The small black spots are voids within the weld that were caused by shrinkage during solidification.

Upon examining the weld closer, as shown in Figure 25, wavy directional lines are observed within the weld pool. These lines indicate microsegregation of chromium-rich and nickel-rich regions. Examination by EDS determined that the average composition of the weld was 10 at% Cr, implying that the alloyed region is within the solid solution limits and well below the chromium concentration where the α-phase should form. An SEM image of the same weld is shown in Figure 26, which shows a clearer image of the microstructure. The presence of microsegregation revealed by polishing with no etching shows that the welds are not in an equilibrium state.

One single weld that contained the full library of compositions from pure nickel to pure chromium was desired, but examination by EDS determined that this was not possible with our equipment and procedures. Each weld was checked by EDS across the surface to determine the composition range. The samples had to be cut in half in order to fit into the SEM, and each half of the sample was examined in at least three places. In each of these examinations, at least three measurements were made and the average concentration was recorded, as shown schematically in Figure 27.

The concentration change showed a linear tendency, as expected, and an example of the concentration gradient is shown in Figure 28. As described above, the full composition range was not obtained, and these three welds only had ranges from 18 to 50 at% Cr. There is significantly more scatter in the data at the thick end of the wedge at concentrations greater than 40 at% Cr, which could be caused by the rougher surface of the weld or by the introduction of a secondary phase. According to the Ni-Cr phase diagram at the 900ºC isotherm, the dual phase region appears around 40 at% Cr. There could also be regions of unmelted chromium film at the thick ends of the wedged film.

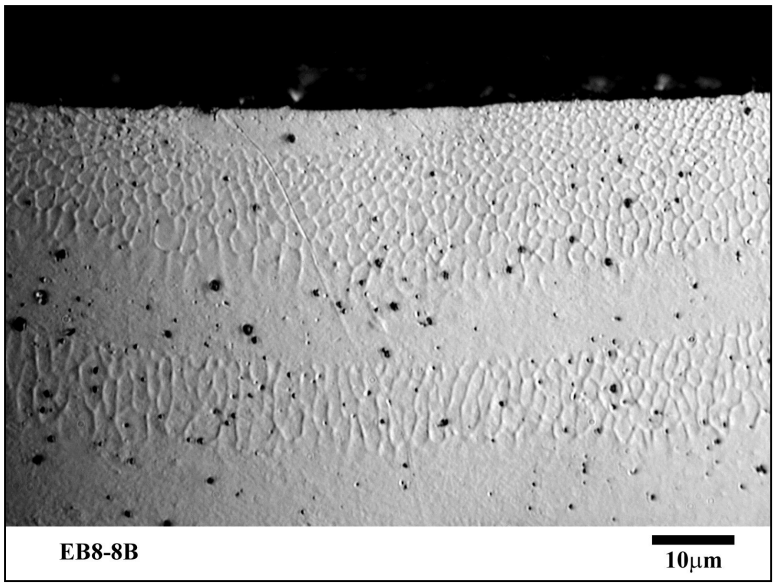

Figure 25: Cross section of EB weld (130kV, 0.7 mA, 10 ipm) at 1000x magnification (concentration of about 10 at% Cr).

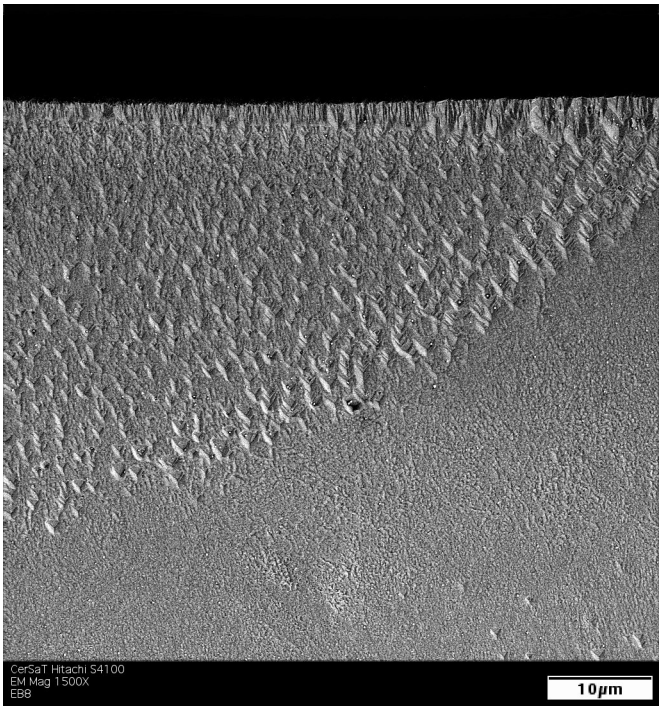

Figure 26: SEM image of EB weld (130kV, 0.7 mA, 10 ipm) at 1500x magnification (concentration of about 10 at% Cr).

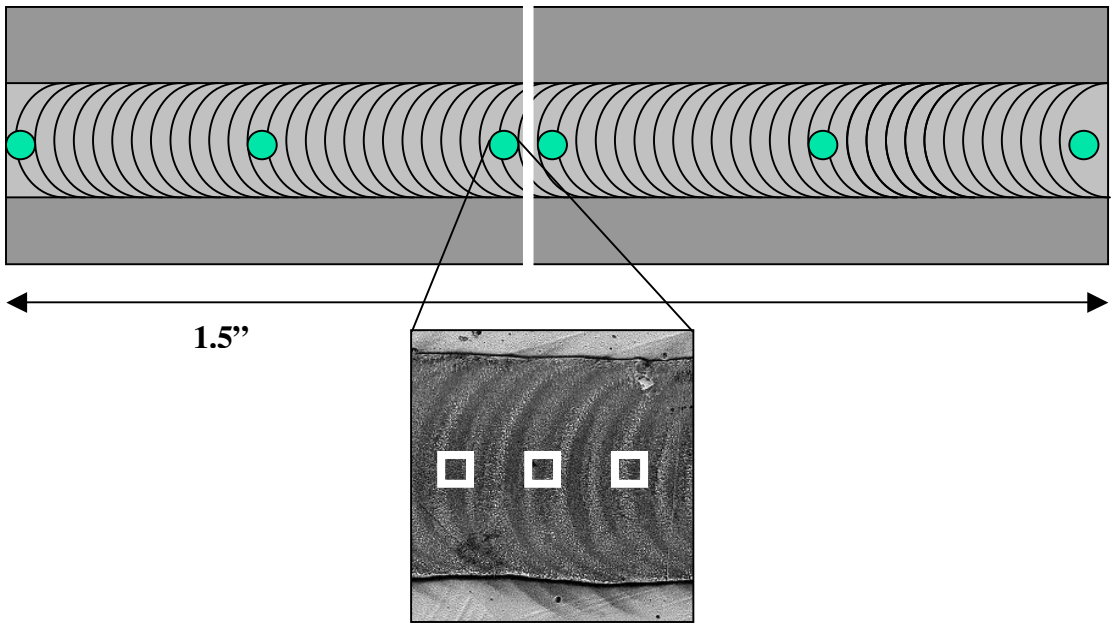

Figure 27: Schematic showing EDS measurements for samples with Cr films on Ni substrates.

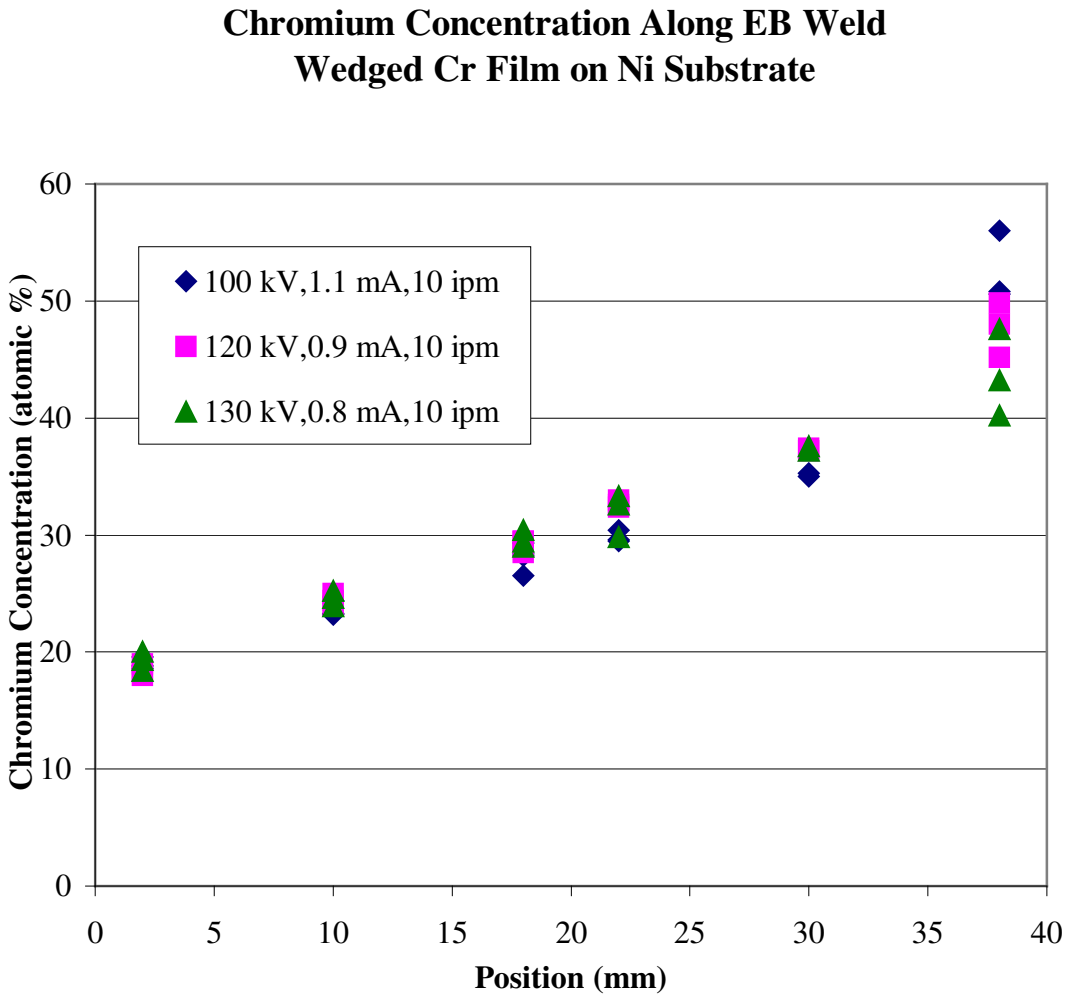

Figure 28: Concentration gradient along length of weld for Cr films on Ni substrates.

Verification of Alloy Uniformity

Though the surface details appeared to show strong tendencies that indicated a true combinatorial alloy library, several tests were performed to verify that these alloys were uniform throughout the weld. First, cross sections were made and the welds were examined by EDS to evaluate the depth of the chromium concentration. Figure 29 shows the concentration profile of a typical EB weld. The top of the cross section had a concentration that was only 2 at% lower than the concentration evaluated from the surface of the weld, indicating that the EDS examinations from the surface were accurate.

The concentration held fairly constant at 26-28 at% Cr to a depth of about 18 μm, which is half of the total weld depth of 37 μm. The weld still had above 20 at% Cr at a depth of 28 μm, and the chromium concentration dropped to 10 at% at the weld pool boundary. The inset in Figure 29 shows the cross section of the weld with the white marks indicating the points of the EDS evaluation.

In addition to the EDS verification, several nanoindentation tests were also performed to examine the uniformity of the welds. Indents were made on the cross section of the weld to determine how the mechanical properties varied through the depth. Figure 30 indicates that the hardness remained fairly constant through most of the depth. Unfortunately, more indents could not be made through the depth in a single weld because the indents must be a certain distance apart to prevent the data from being affected by the deformation caused by the neighboring indent. The cross section shown in the figure had a chromium concentration of 43 at% near the surface of the weld, which was only 2 at% less than the concentration measured at the surface.

More indents were made on the cross-sections to prove that the indentations made on the rough surface would agree with data from the indents on the polished cross sections. Cross sections were made at the ends of a sample, and three welds were examined. Four or five indents were made in each cross-sectional weld, and the hardness values obtained

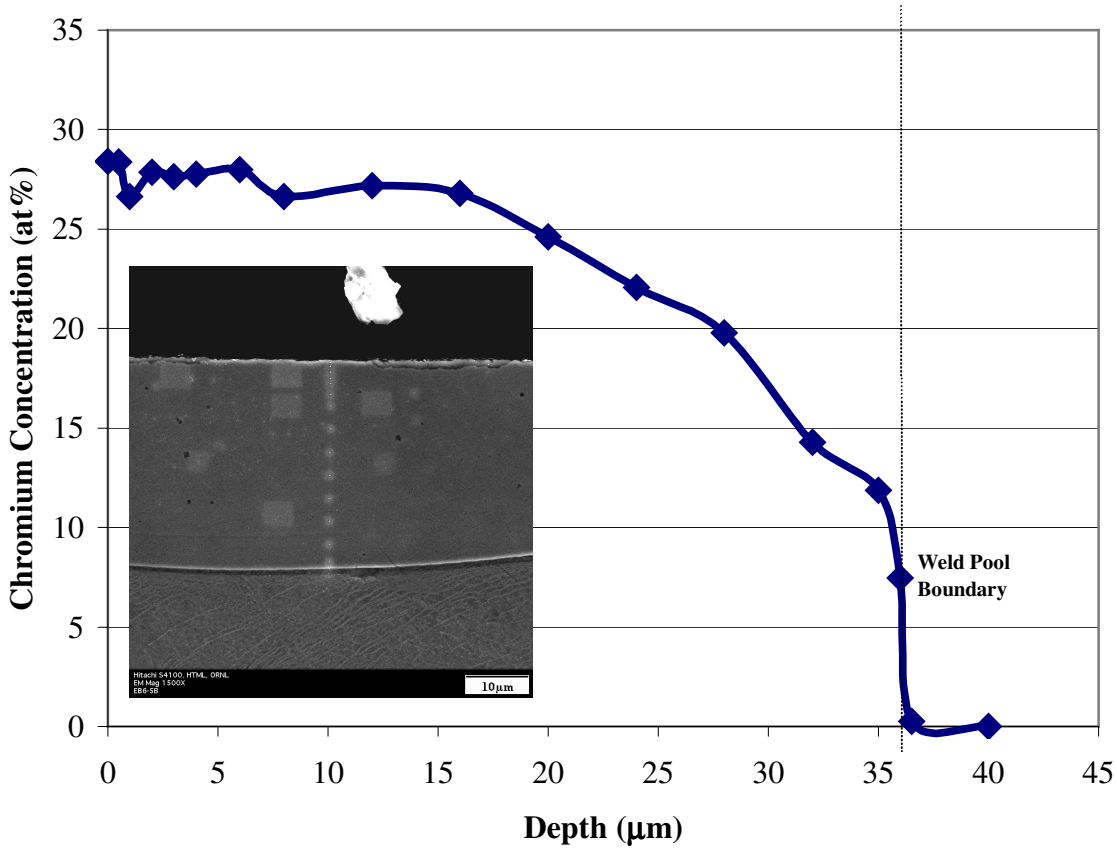

Figure 29: Concentration profile through the depth of EB weld; Cr film on Ni substrate.

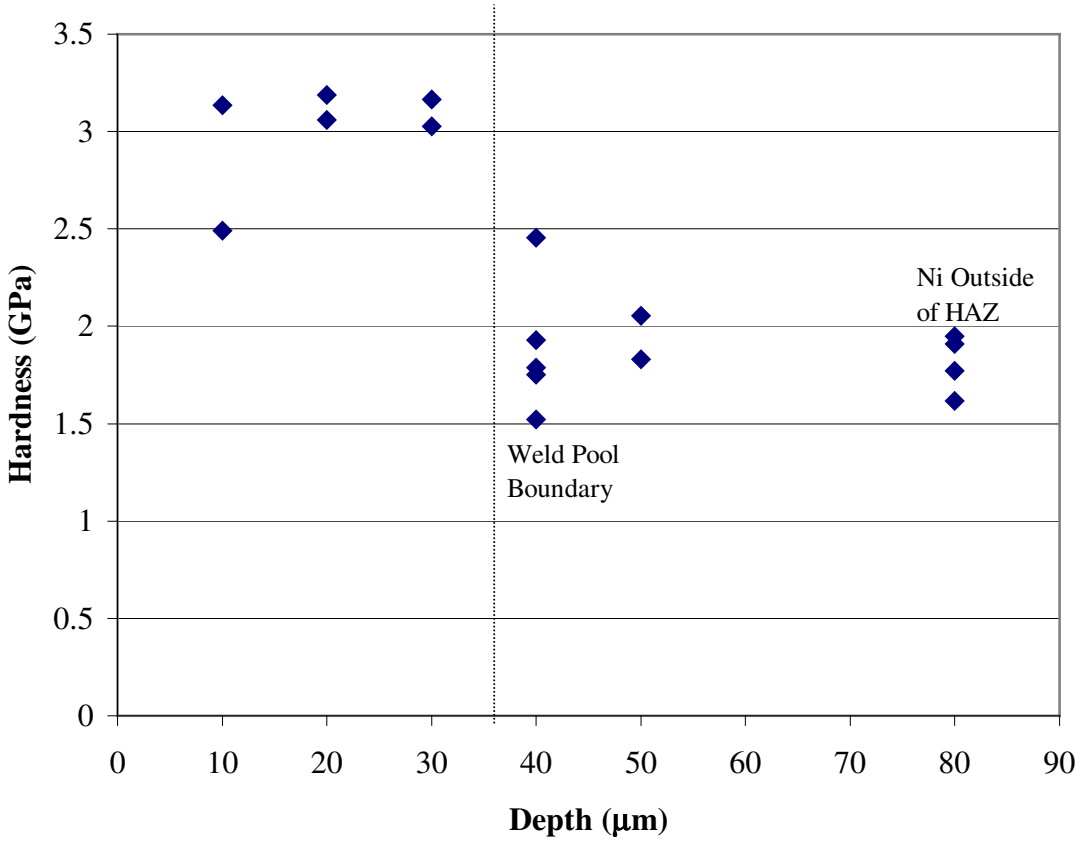

Figure 30: Hardness profile through the depth of EB weld; Cr film on Ni substrate.

were compared to the hardness results taken from the surface. Figure 31 shows the results of the hardness of the cross-sections at each end (blue) compared with the hardness from the surface (red). The inset shows images of the indents taken in the cross-section of the weld pool. The hardness results from the surface compared well with the results from the polished cross-section, showing that the results from the surface adequately represent the true hardness of the weld. This also showed that the surface roughness did not have a significant effect on the results obtained by nanoindentation.

Another type of test was conducted to determine the effect of the surface roughness on the results obtained by nanoindentation. Three different welds with rough surfaces were evaluated by nanoindentation, and then the surfaces were hand polished through 4000-grit silicon paper to reduce the extremely rough surface. Nanoindentation was again performed at the same regions of these three welds, and these hardness results are compared with the original hardness results in Figure 32. The blue points indicate measurements made from the rough surface, and the red points indicate measurements made from the polished surface of the cross section. It can be seen that polishing the surface did little to reduce the scatter of hardness data obtained from the three welds.

These results indicate that the majority of the data scatter cannot be attributed to surface roughness. Another possible contributing factor to the scatter could be voids within the weld caused by the rapid cooling of the weld pool before completely settling from the turbulence of the welding process. The existence of two discreet phases could explain scatter in regions greater than 40 at% Cr, which would also explain why the scatter appears to increase when the chromium concentration is greater than 35-40 at%.

To evaluate the scatter in the data taken from the surface of the welds, a group of six indents was made every 3 mm across the length of the weld, with typical indents made every 800-1000 nm. The group of six indents was made in a 3x2 pattern with 30 μm between indents. The hardness data shown in Figure 33 compares the grouped indents with the typical indents, and the insert shows an image of the 3x2 pattern of indents in

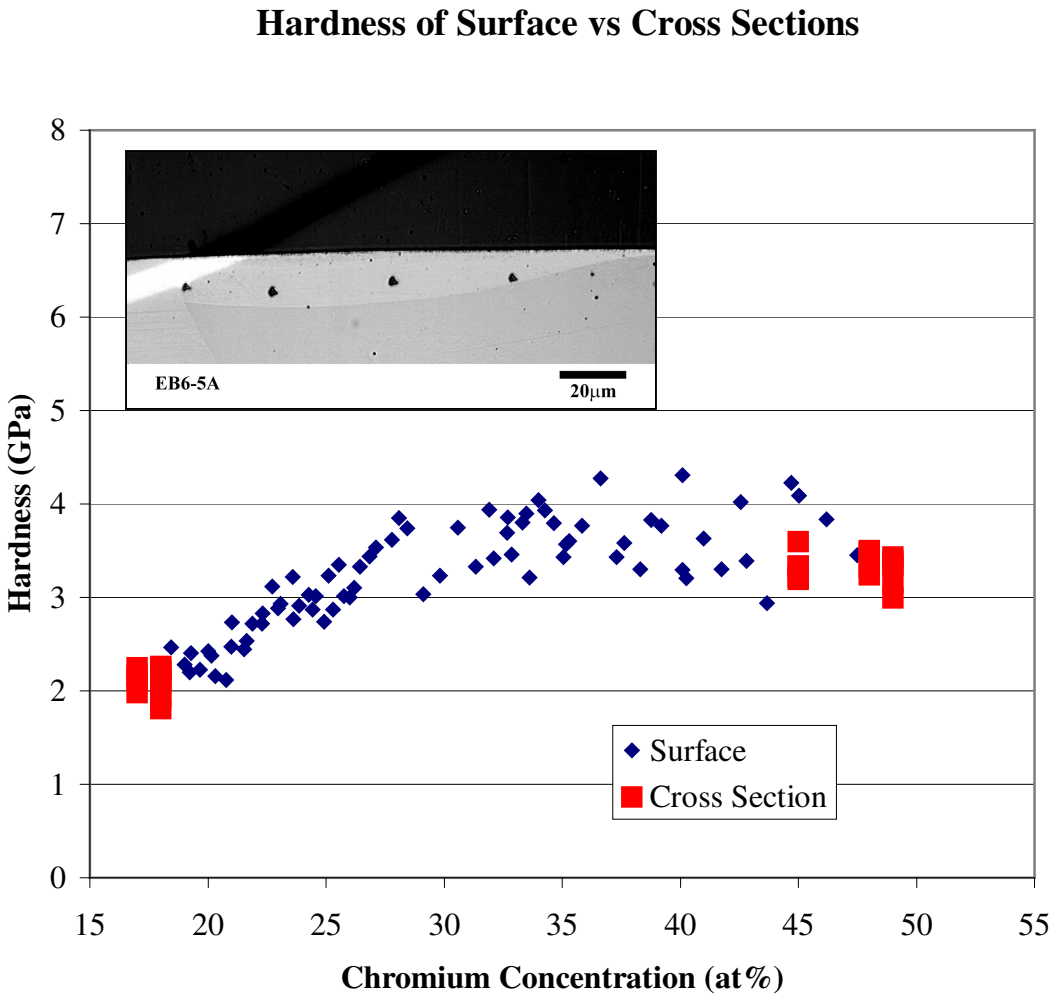

Figure 31: Hardness values for indents taken at surface compared to those taken from polished cross sections at either end.

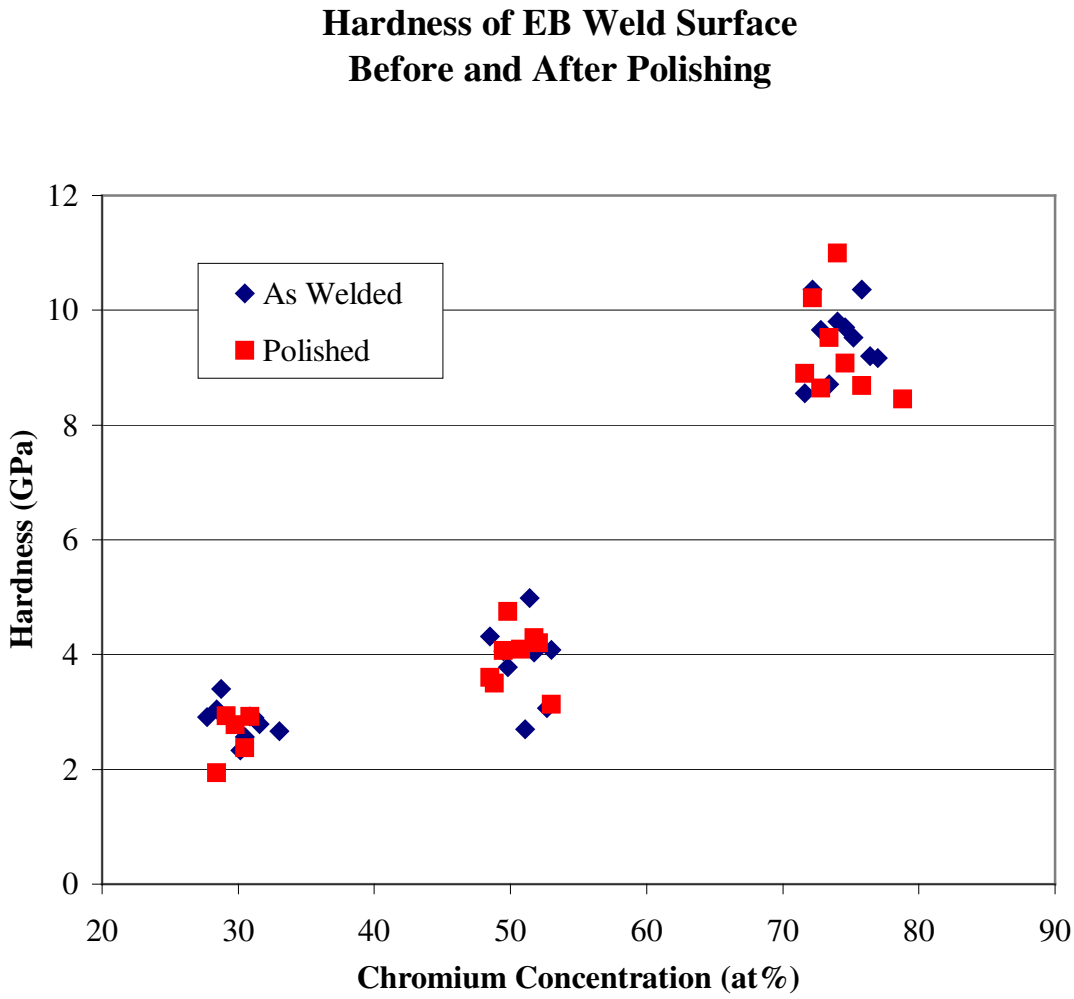

Figure 32: Hardness of EB weld surface before and after polishing.

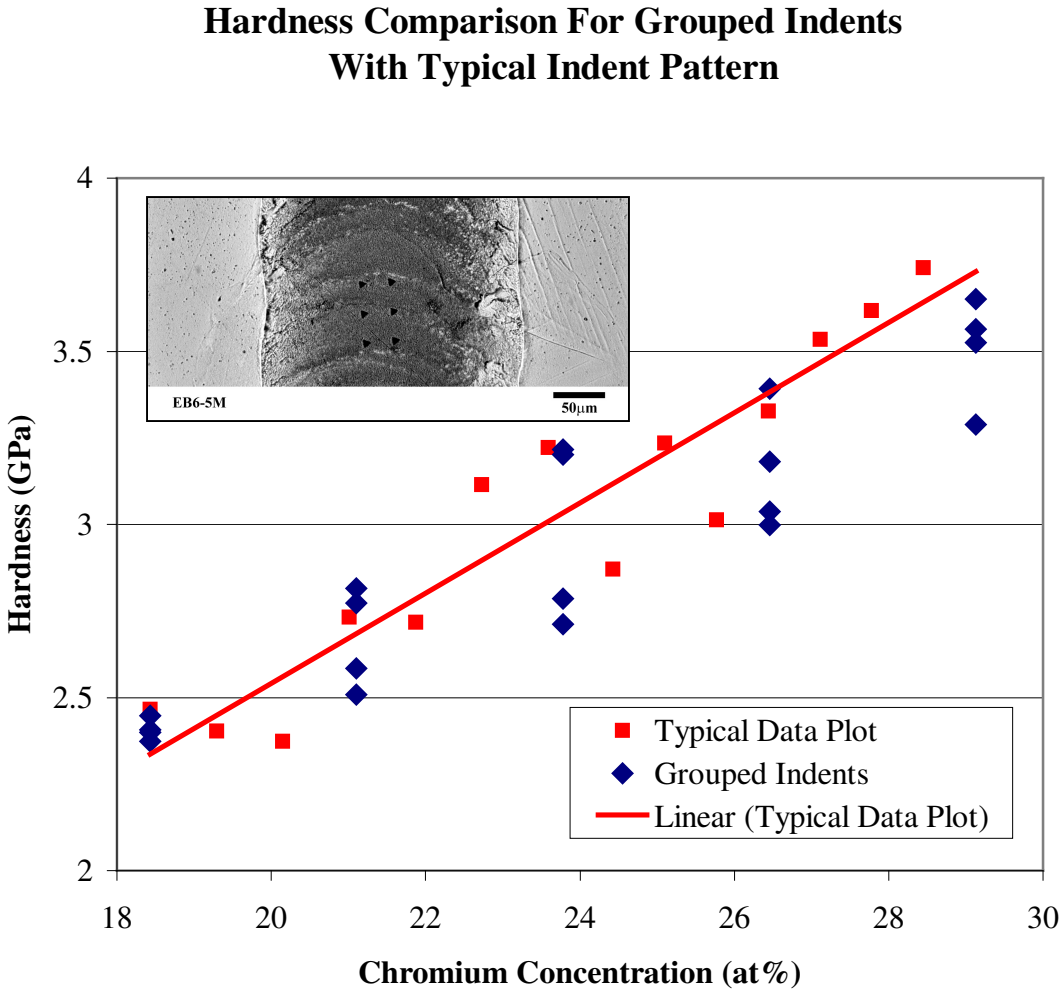

Figure 33: Hardness comparison for grouped indents relative to typical surface measurements.

relation to the surface of the weld. The hardness values for all indents followed the same general tendency. The deviation in each group of six indents shows the typical deviation at any point along the weld. The low hardness deviation of less than 0.4 GPa shows that the welds are uniformly mixed and the indents do not have to be exactly positioned to provide acceptable results.

A series of indents was made perpendicularly across the surface of the weld to examine lateral variations in the hardness measurements. Figure 34 shows a picture of the indents made with the resulting plot of hardness against position. All of the hardness values within the weld pool varied only by 0.5 GPa. The hardness values of 2.5-3.0 GPa within the weld are consistent with the results obtained from other nanoindentations made in regions with concentrations of about 24 at% Cr. The hardness of the chromium film is 7-8 GPa, which is much higher than the 3.8 GPa hardness of the pure chromium cast standard. This higher hardness is explained by microstructure and grain size differences associated with thin films.

Mechanical Properties

Most samples were made with wedged chromium films, but a few were made with flat chromium films. In both cases, adjusting the EBW power parameters had an affect on the resulting concentrations of the weld-produced alloys. The samples with flat films had a uniform concentration through the length of the weld, but those with the wedged film had a concentration gradient through the length of the weld.

Figure 35 compares the weld hardness of a sample with a flat film to welds on a wedged film. The data shows similar tendencies of increasing hardness with increasing chromium concentration. The hardness of the weld on a flat film was higher than the represented weld on a wedged film at 26 at% Cr; however, it was not higher than other welds with wedged films.

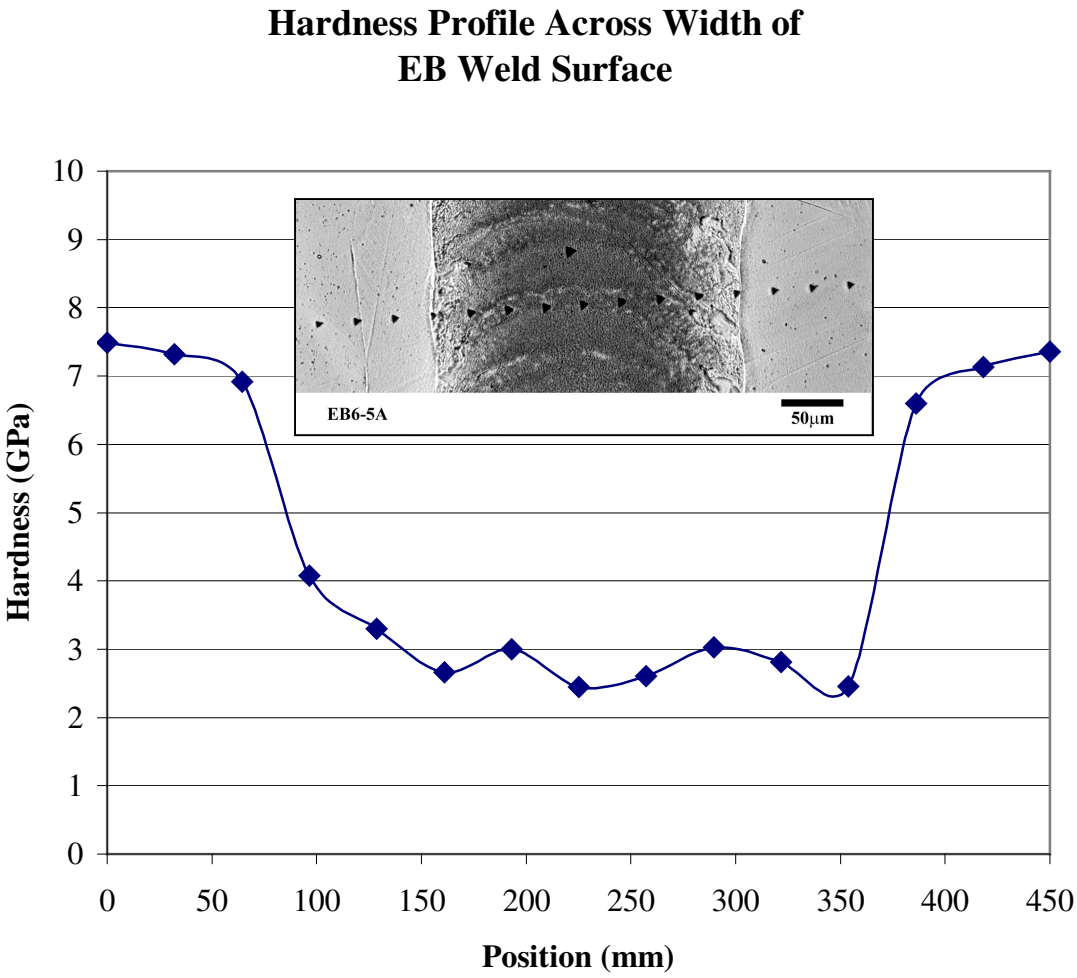

Figure 34: Hardness profile across width of EB weld surface.

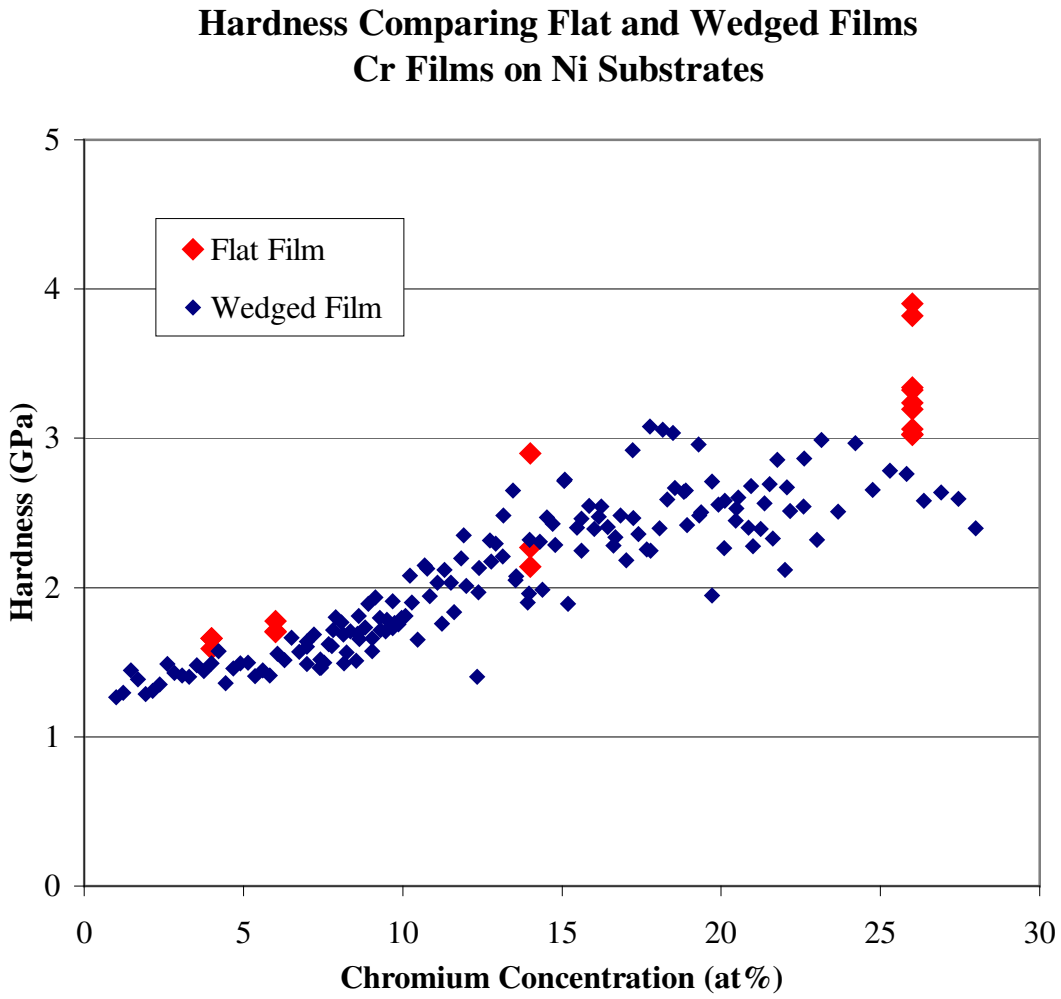

Figure 35: Hardness comparing flat and wedged Cr films on Ni substrates.

Figure 36 compares the elastic modulus of all samples with chromium films on nickel substrates to the Ni-Cr cast standards. Each color of data points represents a different sample with its own series of welds and weld parameters. Most of the modulus values are around 200 GPa, but there is scatter between 150 and 250 GPa.

Figure 37 shows the hardness values of welds with chromium films on nickel substrates. Each color of data points represents a different series weld parameters. The hardness increased with chromium concentration with the same tendency as the cast standards. The initial slope is constant until about 40 at% Cr, where it levels slightly and then increases at a steeper slope than before. This concentration is when a two-phase structure was apparent in the Ni-Cr cast standards. The slight leveling off in slope could be attributed to the low probability of hitting the α-phase at 45 at% Cr. For example, if an isotherm of 900ºC is assumed, then the dual phase region exists between 40 and 95 at% Cr, and there is only 9% α-phase in a Ni-45Cr alloy. The increase in slope after this point is attributed to the greater chance of hitting the α-phase with the indent.

Figure 38 shows the hardness of a sample with a wedged film of chromium ranging in thickness from 2 to 12 μm. The film did not reach a zero thickness due to misalignment of the substrate and shutter during deposition. The sample shows that different EBW parameters can be used to obtain similar results. The welds were able to cover a combinatorial range of 18-52 at% Cr.

Figure 39 shows the hardness of another sample with a wedged film of chromium, but this one with a thickness ranging from 0 to 10 μm. The EBW parameters are similar to those shown in Figure 36, but the ability to reach a zero thickness enabled the missing range of 0 to 18 at% Cr. The reduced total thickness of the film prevented higher chromium concentrations from being obtained, and this sample only covered the combinatorial range of 0 to 28 at% Cr. If this film had been as thick as other specimens, the sample would have covered the whole range between 0 and 52 at% Cr.

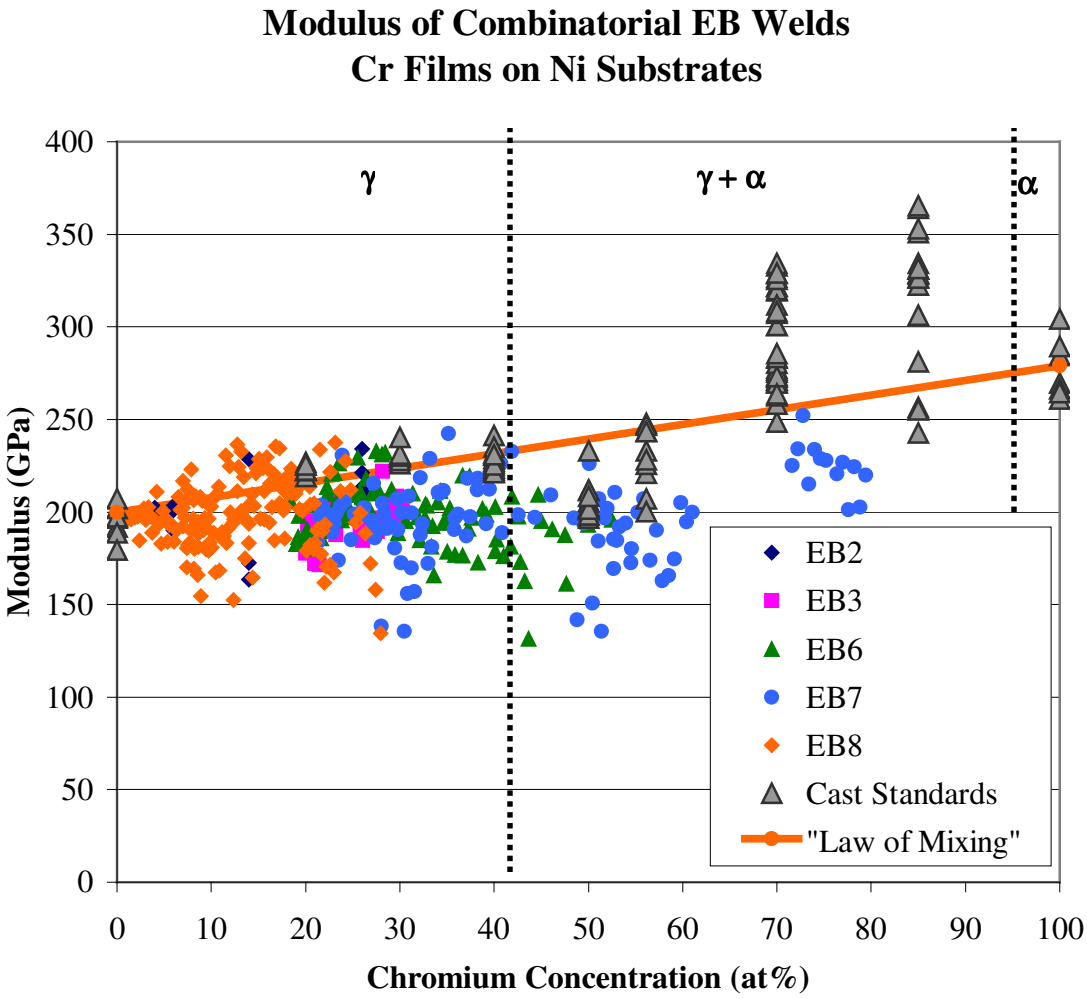

Figure 36: Modulus of all samples with Cr films on Ni substrates.

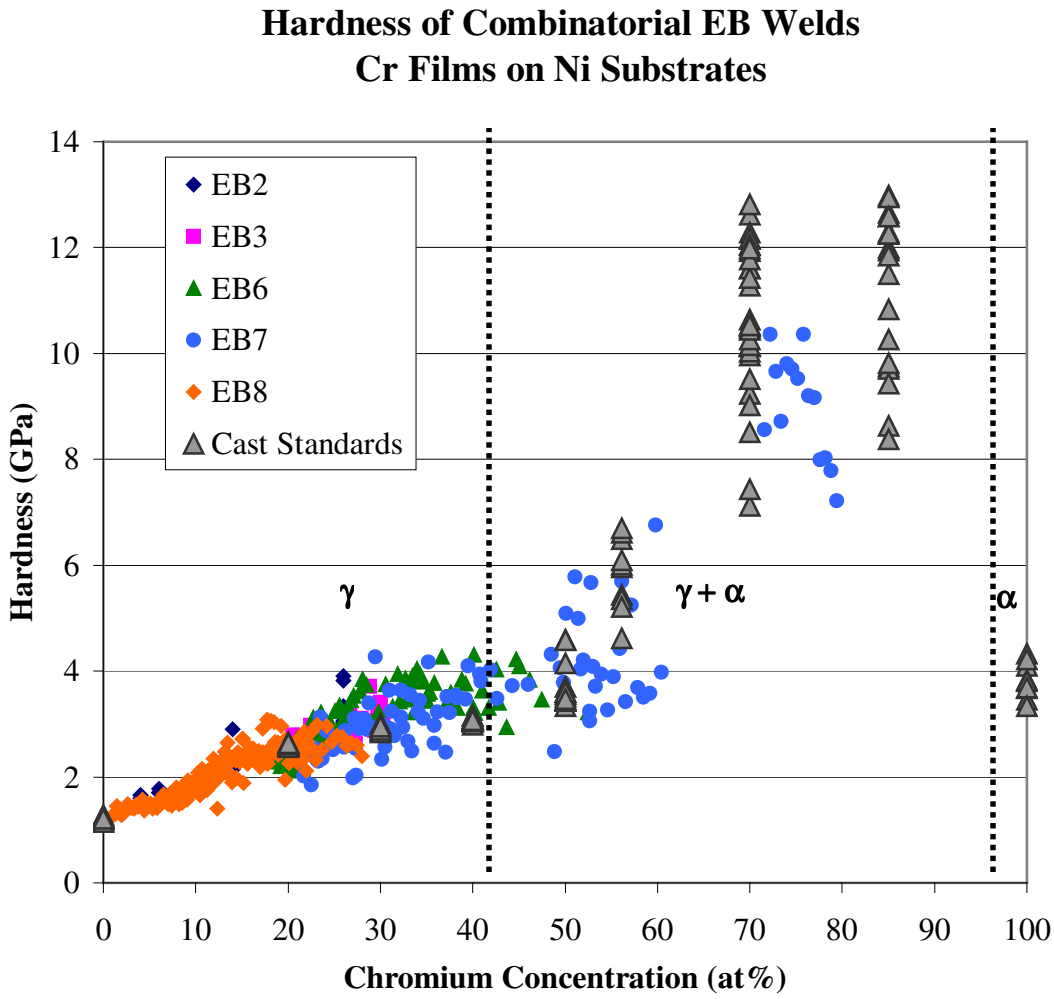

Figure 37: Hardness of all samples with Cr films on Ni substrates.

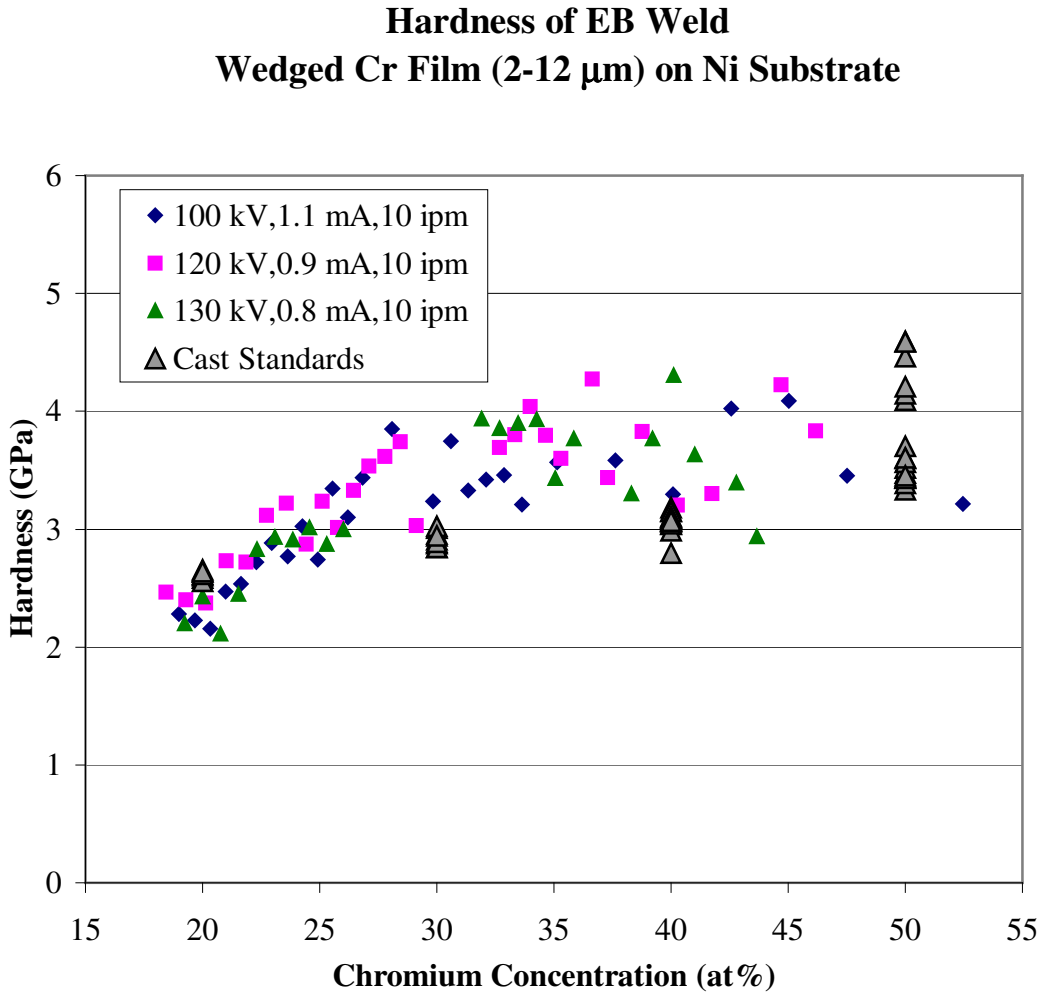

Figure 38: Hardness of EB weld with a wedged Cr film of 2-12 µm on a Ni substrate.

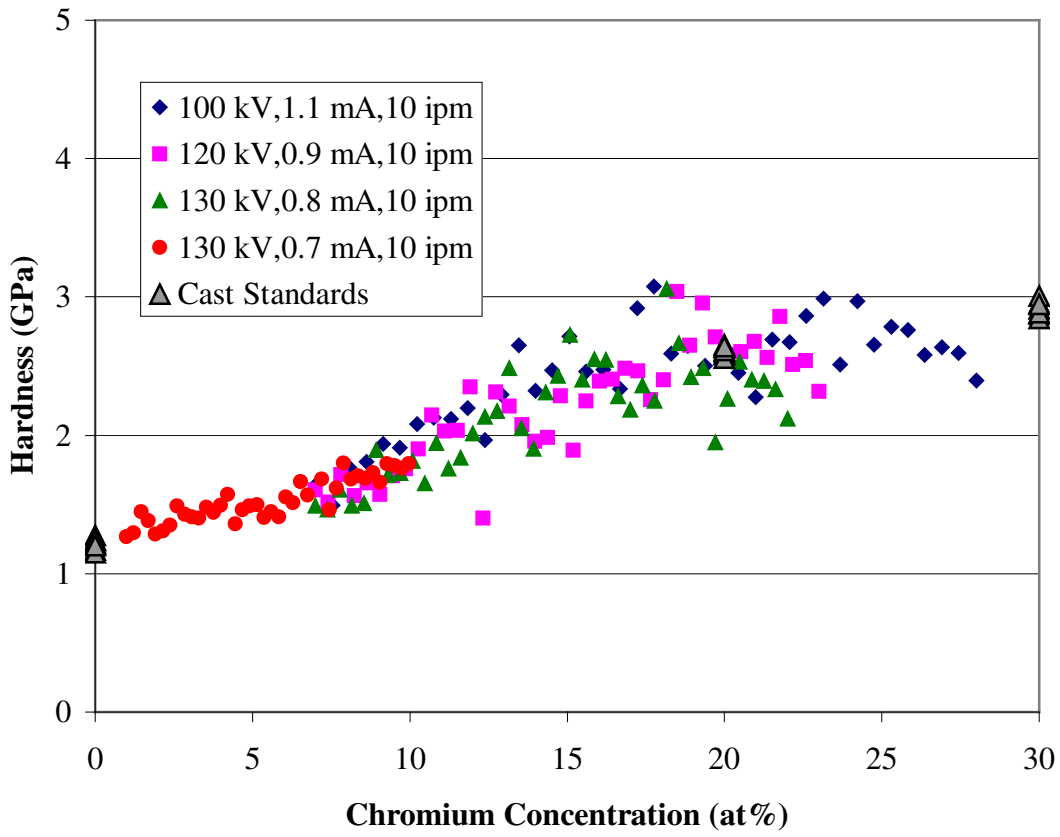

Figure 39: Hardness of EB weld with a wedged Cr film of 0-10 µm on a Ni substrate.

Nickel Films on Chromium Substrates

Only two samples were made, with the successful EBW parameters from the samples with the nickel substrates used in their synthesis. One sample used an accelerating potential of 100 kV, and the other sample used an accelerating potential of 120 kV. Both samples employed a constant travel speed of 10 ipm, and only the current of the EB weld was varied to create the different compositional ranges.

The nickel films did not adhere well to the chromium substrates, especially at the end of the wedge where the thickness was greatest. Since the substrates were made with smaller dimensions, the samples did not have to be cut in half in order to be examined in the SEM or nanoindenter. Figure 40 shows an example of a completed weld sample.

Figure 41 shows a typical top view of the EB welds created from the samples with chromium substrates. Figure 42 shows similar images taken with the SEM. Almost all of the welds made on the chromium substrates had large cracks visible on the surface. Figure 43 shows a cross-section of a weld that shows the depth of one of the cracks through the center of the weld. The large dark spots in the weld are voids, and between the voids can be seen a distinct segregation of phases throughout the weld.

The samples were cross-sectioned at the ends of the welds, and Figure 44 shows an optical image of a cross-section at the thick end of the wedged nickel film after it was etched with glyceregia. It was again observed that the welds with the higher currents were deeper than those with the lower currents, and the deeper welds had a higher chromium concentration. The glyceregia attacked these welded samples much more rapidly than the samples with chromium films on nickel substrates, and the voids in the welds were very apparent. The SEM images shown in Figure 45 show another weld, and the two phases are more easily distinguished in the image on the right. The dark regions are the chromium rich α-phase, and the light regions are the nickel rich γ-phase. The two phases are apparent throughout the weld, from the surface to the bottom of the weld pool.

Figure 40: A finished Cr substrate sample with eight combinatorial EB welds across the length of the wedged Ni film.

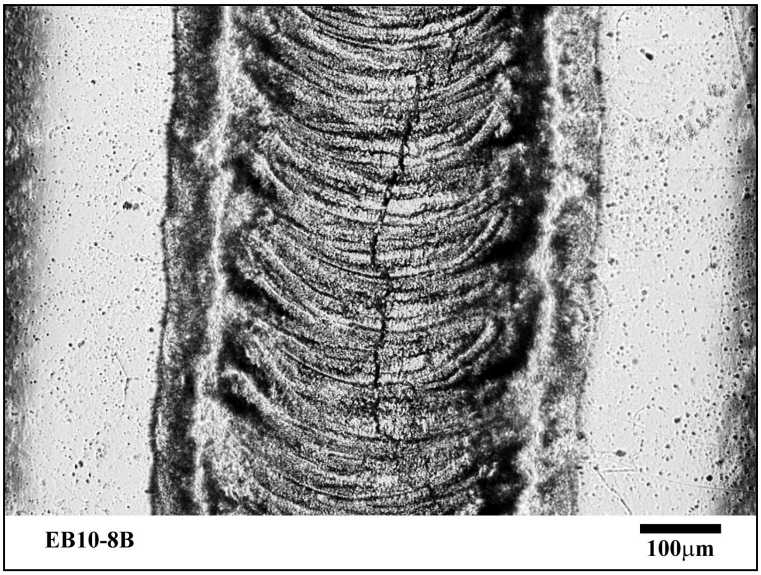

Figure 41: Optical micrograph of surface of EB weld for sample with Ni film on Cr substrate (100 kV, 1.6 mA, 10 ipm).

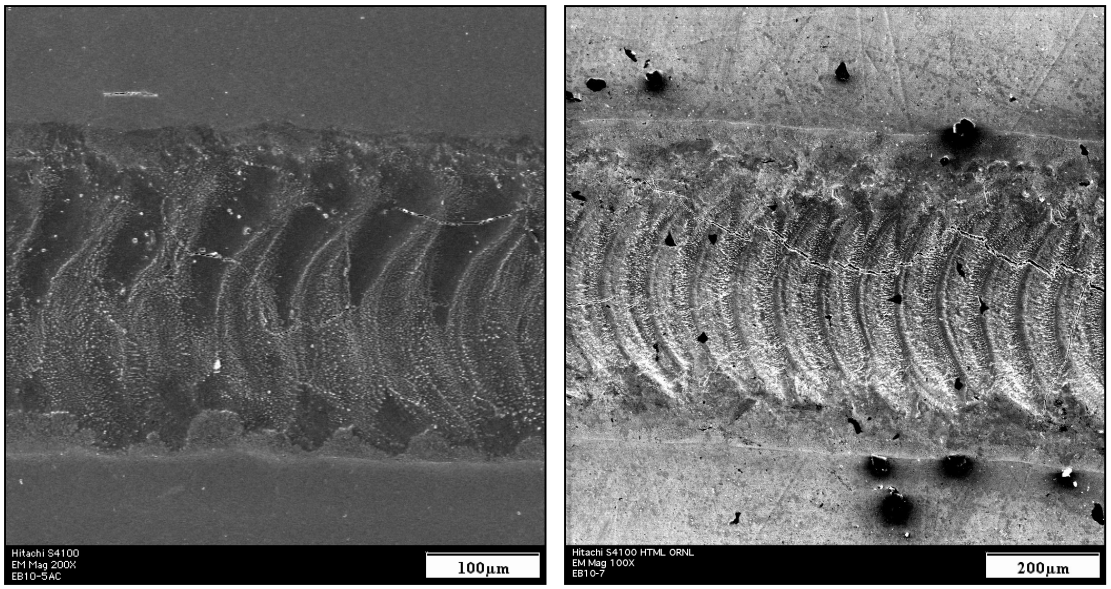

A B

Figure 42: SEM images of the surface of EB welds of samples with Ni films on Cr substrates; A) 100 kV, 1.3 mA, 10 ipm; B) 100 kV, 1.5 mA, 10 ipm.

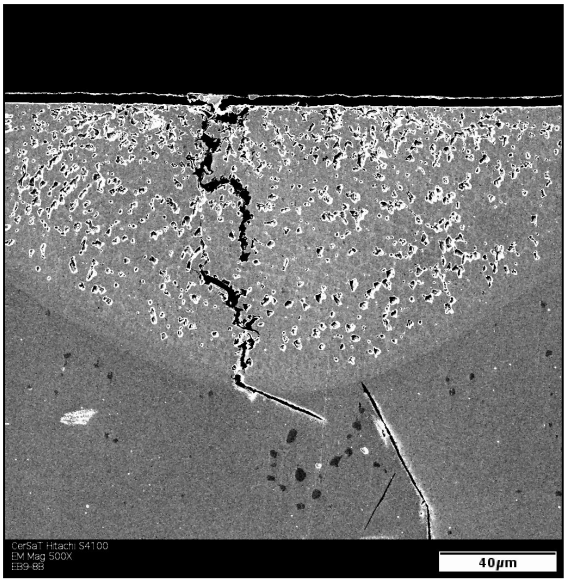

Figure 43: SEM image showing the cross section of a weld with a crack through the center (120 kV, 1.3 mA, 10 ipm; concentration of about 85 at% Cr).

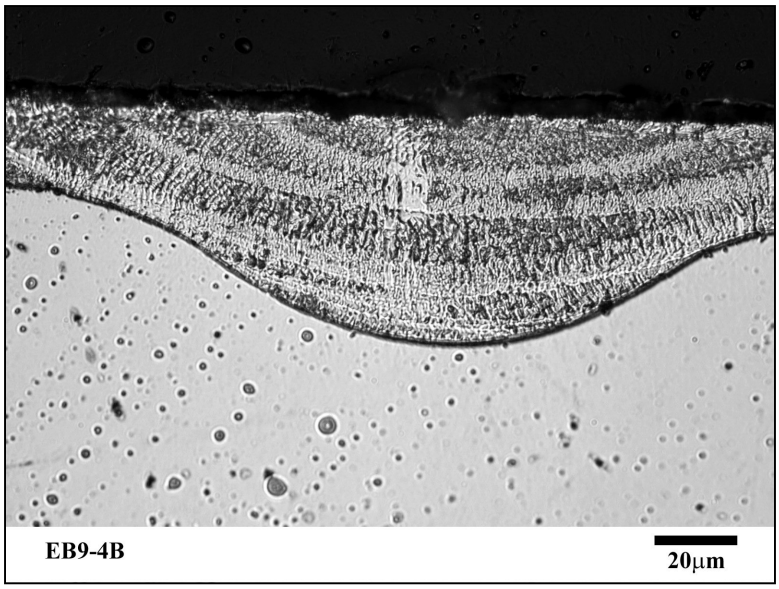

Figure 44: Optical image of a cross-section of an EB weld on a sample of a Ni film on Cr substrate (120 kV, 0.9 mA, 10 ipm; concentration of about 52 at% Cr).

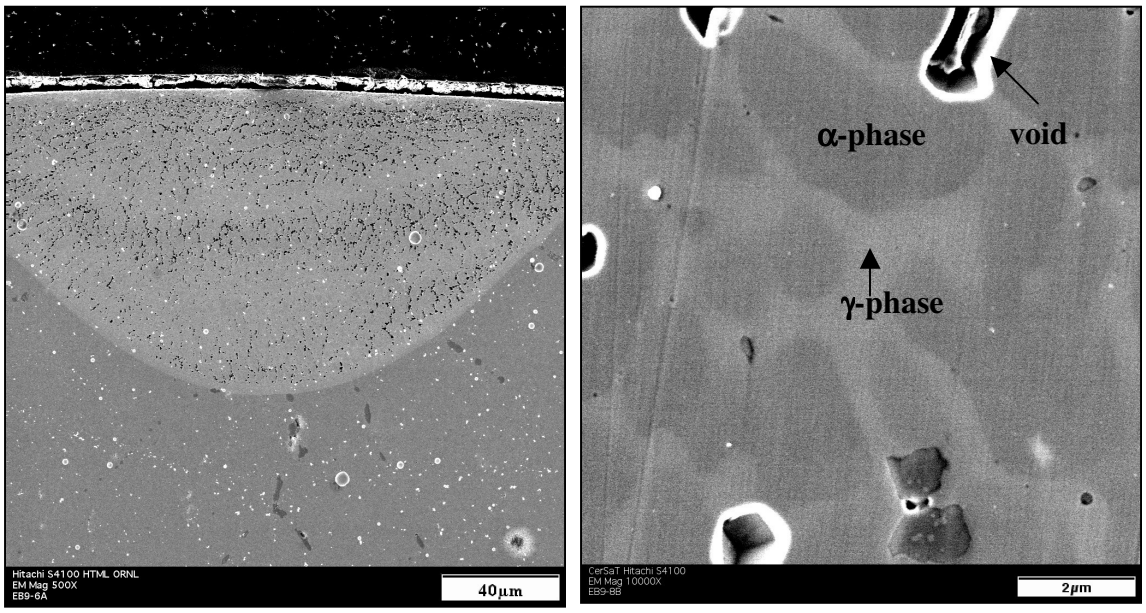

Figure 45: SEM images of cross sections of EB welds (concentration of about 65 at% Cr).

Each weld was checked by EDS across the surface to determine the composition changes due to the nickel wedged film. Each weld was examined in at least five places, and in each of these examinations at least three measurements were made and the average concentration was recorded, as shown schematically in Figure 46.

The concentration gradient of three welds is shown in Figure 47. The welds were all made on the sample with 100 kV accelerating potential and travel speed of 10 ipm. Overall, the chromium concentration did not vary much with position along the weld. The weld produced with a current of 1.4 mA showed the largest changes. The weld produced with a current of 1.3 mA showed a very low chromium concentration at the 7 mm mark. It is uncertain if this region had a high concentration of γ-phase or if there were regions of unmelted nickel film. Overall, this series of welds captured only the combinatorial range from about 70 to 95 at% Cr.

Verification of Alloy Uniformity

Many of the tests to verify uniformity of the samples with nickel substrates could not be used for the samples with chromium substrates because of the presence of dual phases. As can be seen in Figure 45, the welds created on the chromium substrates had finely intermixed regions of γ-phases and α-phases, each with distinctly different properties.

As with the samples on the nickel substrates, cross-sections of the welds were examined by EDS to evaluate the depth dependence of the chromium concentration. Figure 48 shows a typical concentration profile. The top of the cross section had a concentration that was only 5 at% lower than that evaluated on the surface of the weld, indicating that the EDS examinations from the surface were accurate. However, the concentration did not vary smoothly through the depth of the weld due to the separation of the two phases.

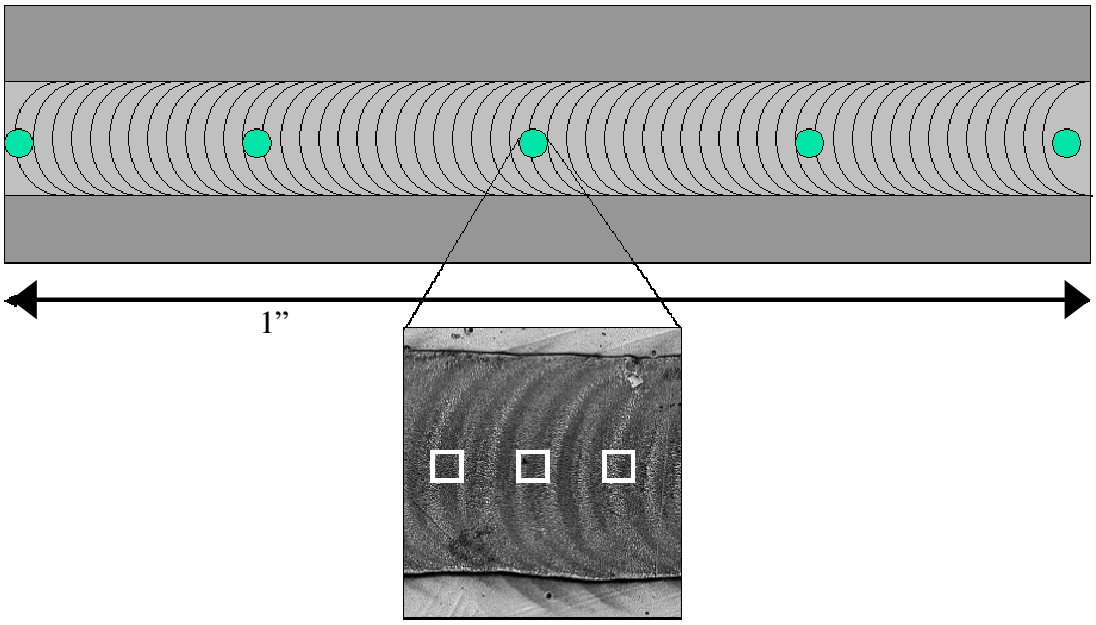

Figure 46: Schematic showing EDS measurements for samples of Ni films on Cr substrates.

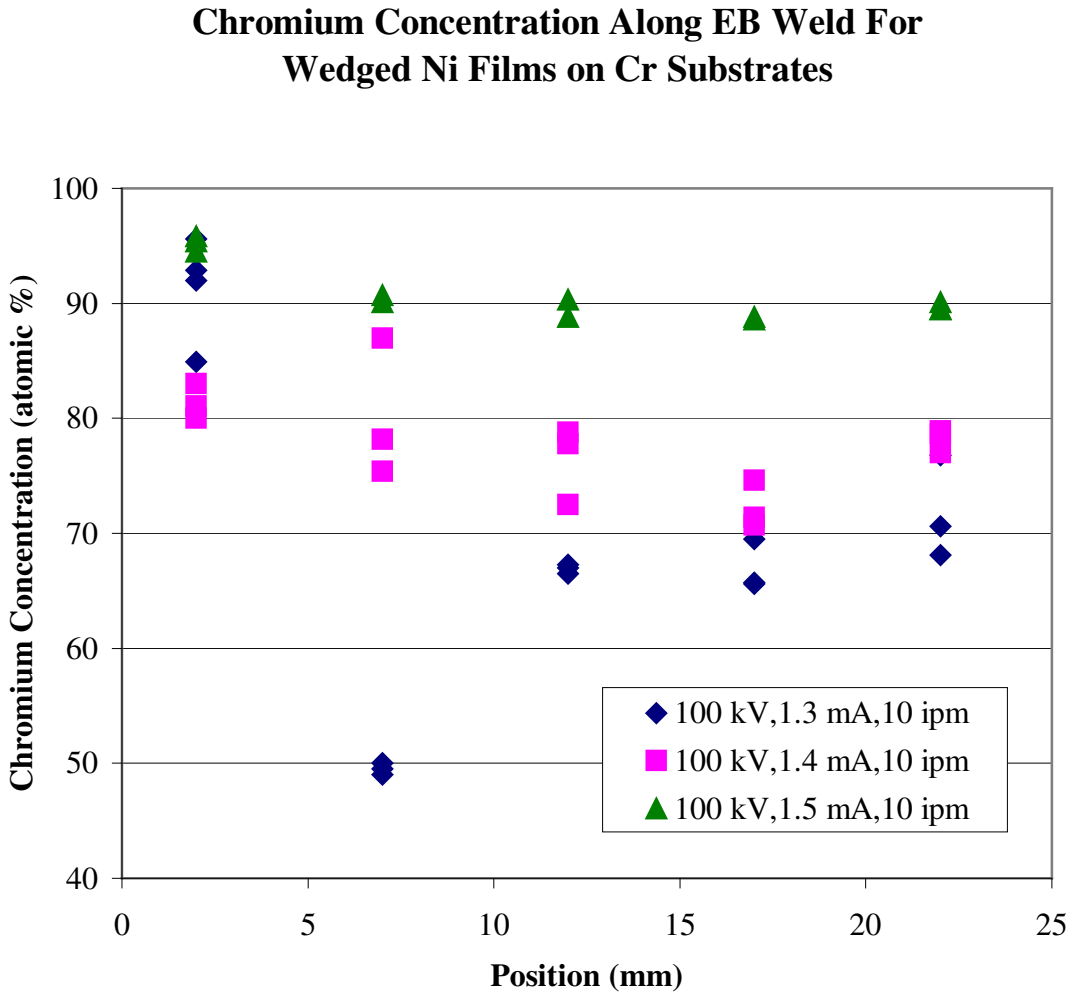

Figure 47: Concentration gradient along length of weld for Ni films on Cr substrates.

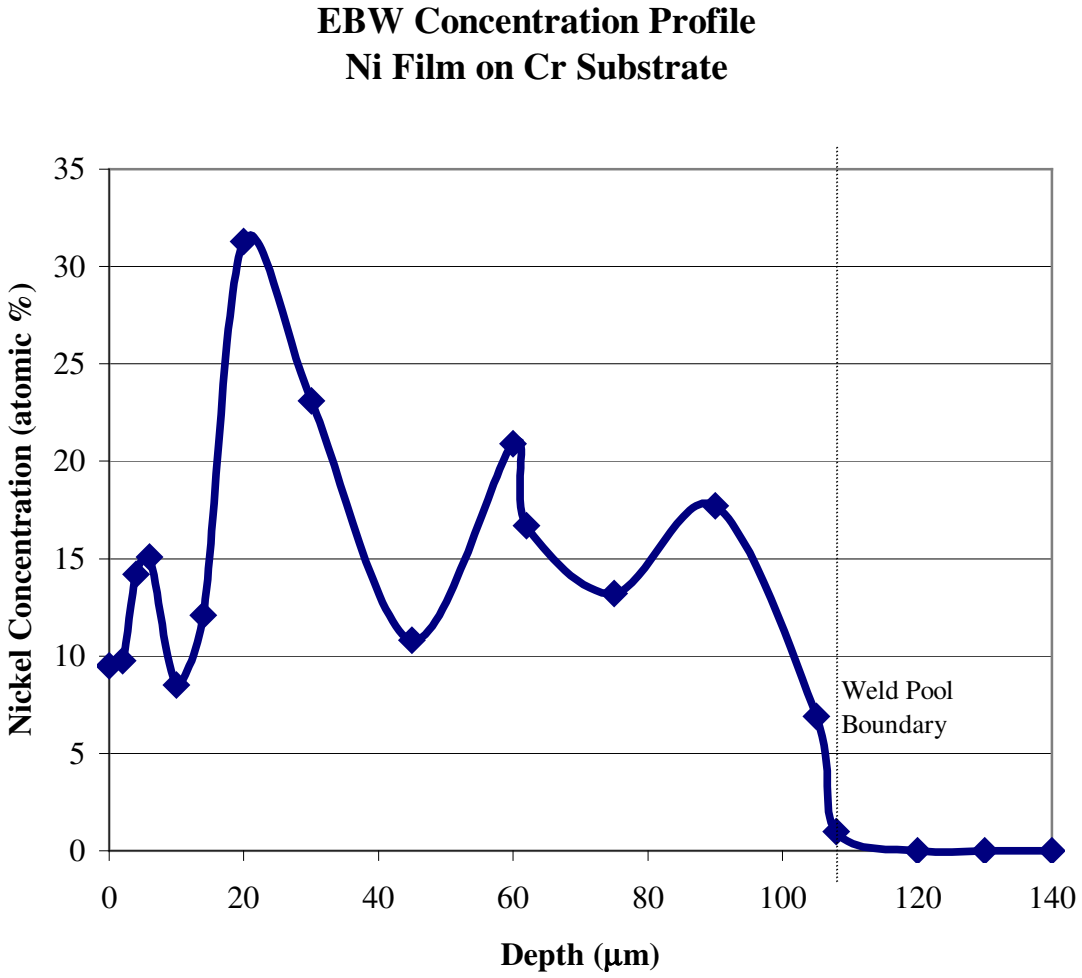

Figure 48: Concentration profile through depth of EB weld; Ni film on Cr substrate.

Mechanical Properties

The modulus and hardness of the samples were evaluated for both samples made with Ni films on Cr substrates. Due to the cracks produced in many of the welds, several of the indents made by the standard tests described earlier produced no data. This was particularly prominent for the sample made with an accelerating potential of 100 kV. In order to establish measurable data from the welds, individual indents were made at specific points along the weld, being careful to avoid the fine cracks and rough surface. Before indentation, the NanoII system was calibrated twice to ensure accuracy and precision of the indent positions.

The modulus results for both samples are shown in Figure 49. The samples made with an accelerating potential of 120 kV are shown in blue and the samples made with an accelerating potential of 100 kV are shown in magenta. There is a large scatter in this data, which can be explained by the high frequency of cracking as well as the dual phases observed in the welds. Some of the modulus values were above 279 GPa (modulus of pure chromium), though most were within the 10% deviation allowed by the nanoindentation results, and all were lower than the upper constraint provided by the Ni-70Cr and Ni-85Cr cast standards. Most of the modulus results were below the "law of mixing" line, but most of these data points were above the lower limit provided by the Ni-50Cr and Ni-56.14 cast standards.

The hardness values are shown in Figure 50. The hardness data showed trends similar to the data from the cast standards, but because of the large scatter of data due to the dual phases and the high occurrence of cracking, it is difficult to make specific trend distinctions. The hardness values between 70 and 85 at% Cr are almost all between the hardness values of the Ni-70Cr and Ni-85Cr cast standards. There are a few hardness values less than those for the standards, but these are still higher than the hardness values for the Ni-50Cr standard, where the nickel rich γ-phase is assumed to be a fully saturated solution.

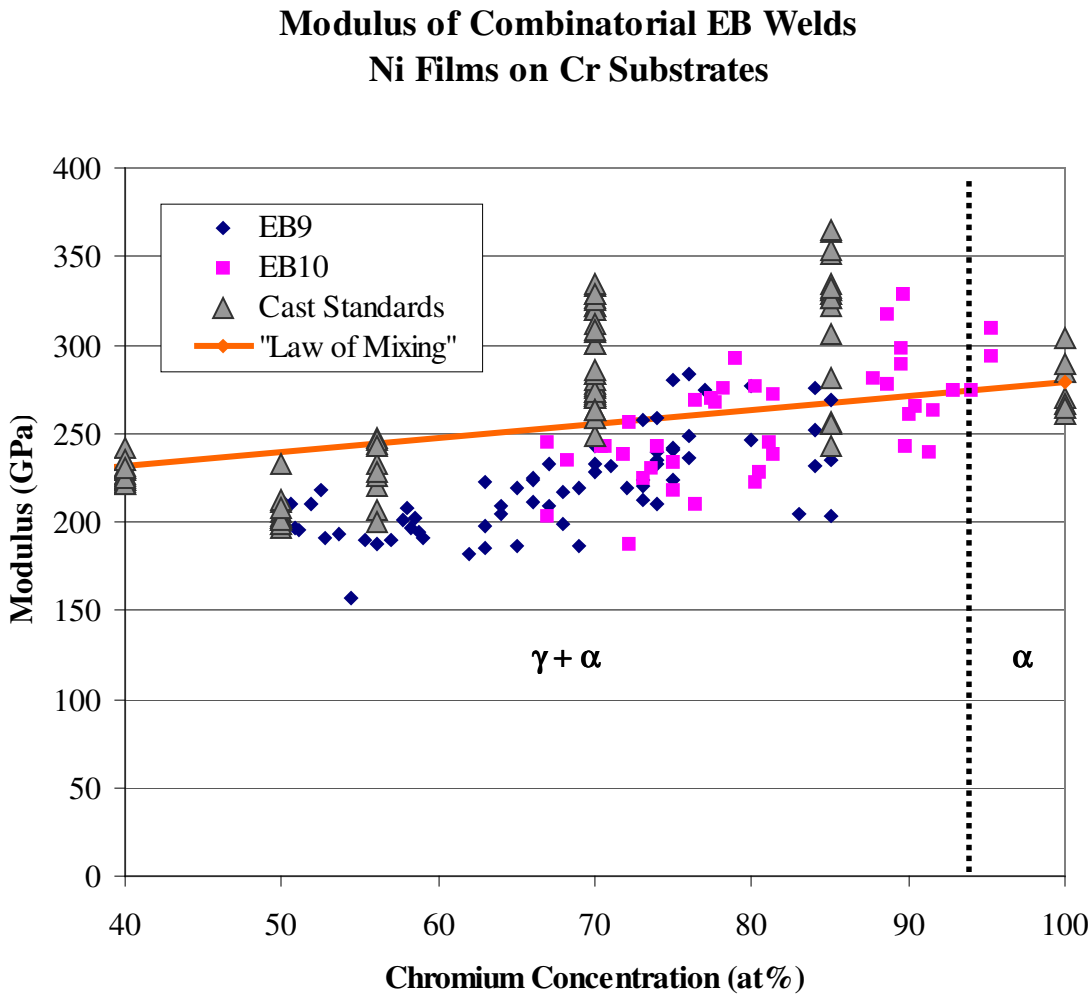

Figure 49: Modulus of combinatorial EB welds for Ni films on Cr substrates.

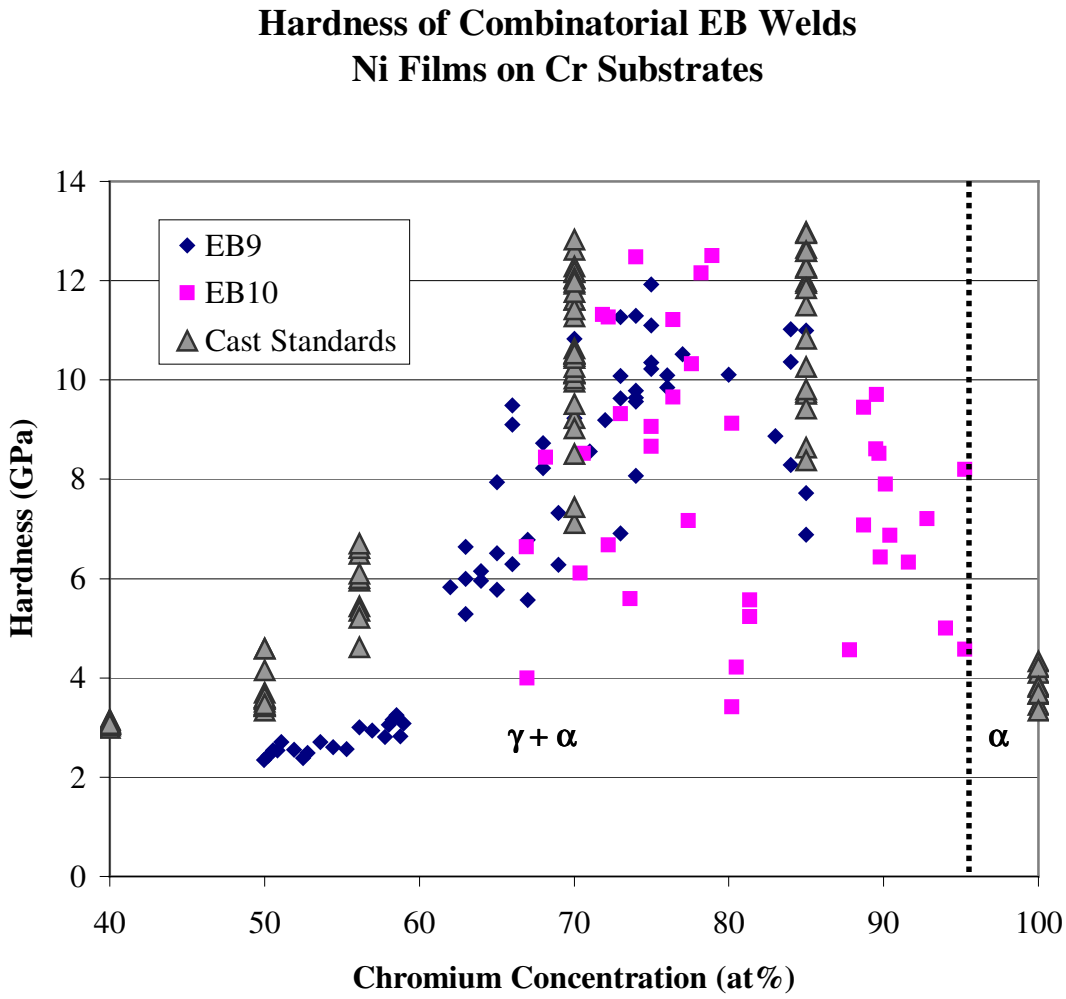

Figure 50: Hardness of combinatorial EB welds for Ni films on Cr substrates.

It was difficult to obtain results from the end of the weld with greater than 90 at% Cr, and the compositional range above 95 at% Cr was not achieved. Therefore, there is not a clear understanding of trends greater than 90 at% Cr, and hence there is no specific evidence to what happens at the solution saturation point of the α-phase. Of the few data points acquired in this region, all fall below a hardness value of 9 GPa. Since the saturated α-phase is assumed to have the highest hardness values measured (nearly 13 GPa), it is assumed that the saturation point of the α-phase is between 80 and 90 at% Cr where only a few hardness values reached 11 GPa. According to the phase diagram, it would then be assumed that temperatures reached at least 1100ºC before rapidly cooling to retain that microstructure.

Combined Ni-Cr Combinatorial Samples

Considering all the samples that were made with chromium films on nickel substrates and the samples that with nickel films on chromium substrates, the EB welds were able to produce a combinatorial alloy range of 1 to 95 at% Cr. There were only a few gaps in the composition range that were not covered, although it was much more difficult to produce a complete compositional gradient on the samples with the chromium substrates.

The combined results for the modulus of the Ni-Cr combinatorial alloys are shown in Figure 51. The results coincide with the "law of mixing" line until almost 40 at% Cr, and then the modulus values are lower than the "law of mixing" for chromium concentrations between 40 and 80 at%. However, the modulus values from the Ni-50Cr and Ni-56.14Cr cast standards were also lower than the "law of mixing" values.

The hardness values for all of the Ni-Cr combinatorial alloys are shown in Figure 52, along with an insert of the Ni-Cr phase diagram. The hardness results generally coincide well with the hardness of the cast Ni-Cr standards. As with the cast standards, the hardness of the combinatorial welds increased linearly from 1.2 to 3.5 GPa with little deviation from 0 to 40 at% Cr. From 40 to 50 at% Cr the hardness remained steady at

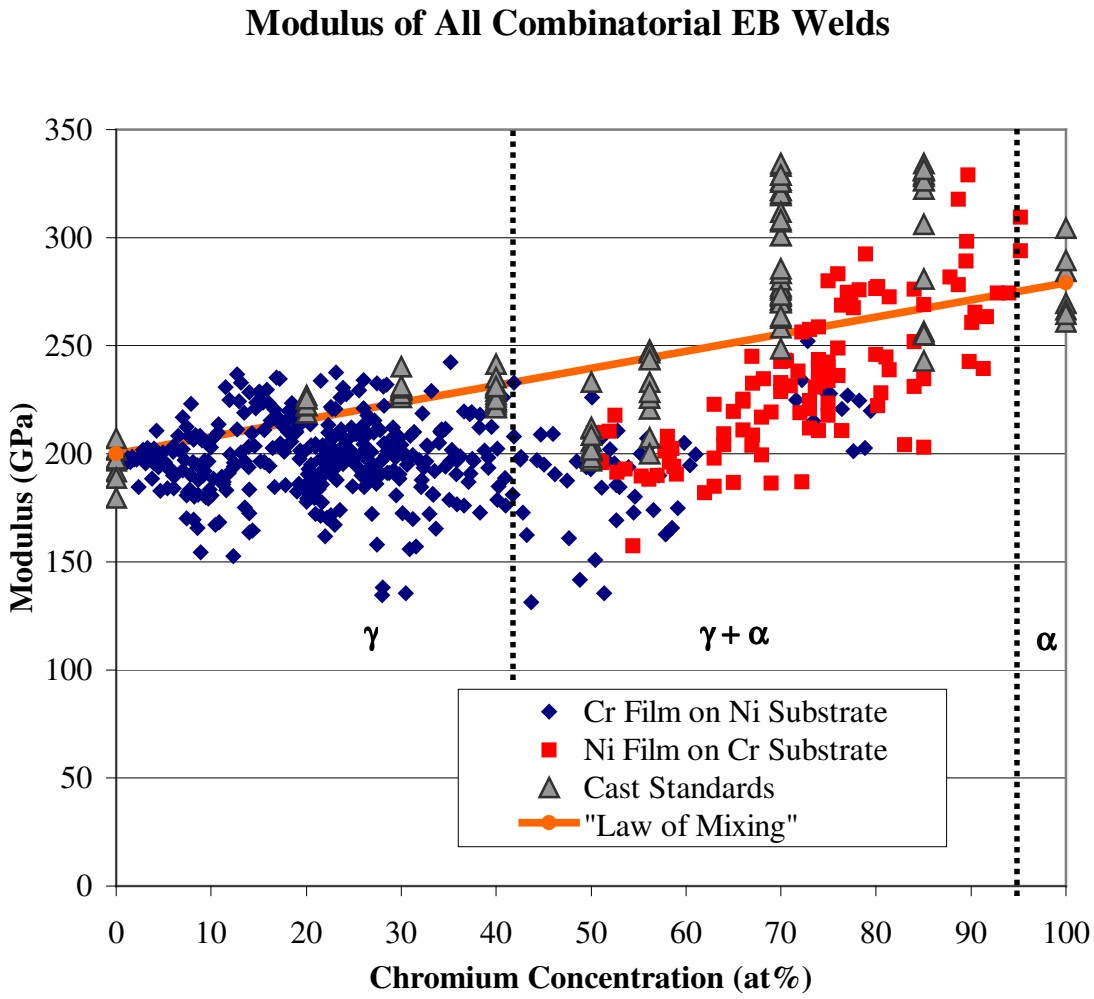

Figure 51: Modulus of all combinatorial EB welds.

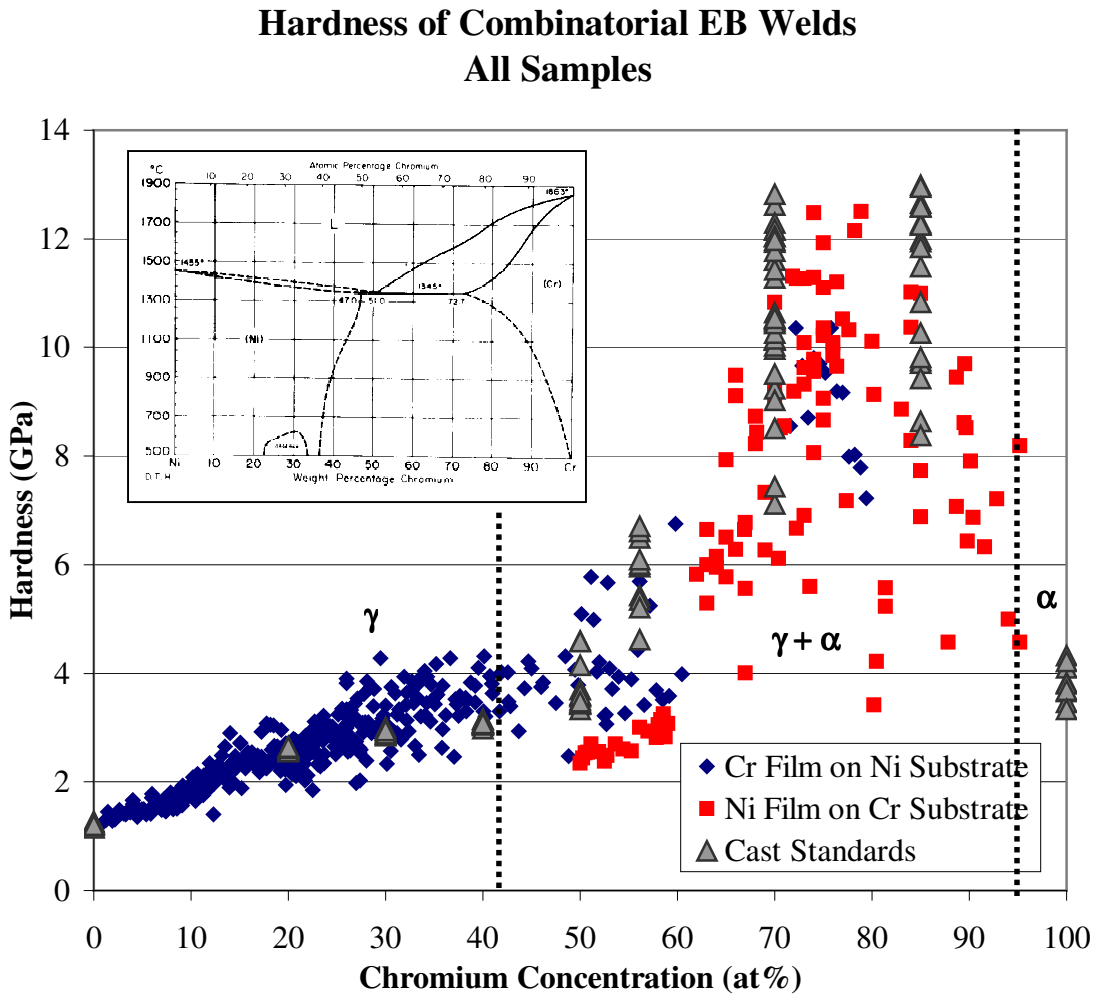

Figure 52: Hardness of all combinatorial EB welds.

about 3.5 GPa, and then greatly increased to values between 6 and 13 GPa from 70 to 85 at% Cr. This high hardness is attributed to the chromium rich α-phase, and the large scatter at this composition is due to the difference in hardness between the γ-phase and α-phase in this dual phase region. Although there is not enough data to make a conclusive argument, it appears that the hardness values begin to decrease after about 85 at% Cr toward the hardness value of pure chromium, which was about 3.8 GPa.

For the samples of chromium films on nickel substrates, there was only one weld that produced adequate results above 60 at% Cr. This weld had chromium concentrations between 71 and 80 at%. All of the values from this weld fell between the hardness values of the Ni-70Cr and Ni-85Cr cast standards, and they are presumed to be just as accurate as the data obtained from the welds on chromium substrates at these compositions.

Chapter 4: Conclusions

The combinatorial method of vapor deposited films alloyed with bulk substrates by EB welding showed promise for the nickel-chromium binary alloy system. There was a linear gradient of composition along the length of the welds that could be easily measured from the surface. The mechanical properties of hardness and modulus obtained by nanoindentation could also easily be characterized from the surface of the rough welds. Both the mechanical and compositional measurements were representative of the measurements taken from the more polished and uniform cross sections.

The cross sections of the EB welds showed segregation and phase transformation comparable to those exhibited by the cast Ni-Cr standards. The compositions of the alloyed weld pools remained relatively constant through at least half the weld depth, which was more than thirty times the depth of the nanoindentation taken from the surface.

There were no strong tendencies shown in the modulus measurements, and the scattering of modulus results limited any conclusive correlations about various composition changes. However, all of the modulus values were within reasonable deviation from the standards set by cast Ni-Cr alloys, though most fell below the linear "law of mixing" value.

There were strong trends in the hardness measurements that followed similar tendencies of the standard Ni-Cr alloys prepared by melting and casting. The hardness values also showed trends that coincided with the composition changes associated with the Ni-Cr phase diagram. The hardness results obeyed a clear trend in the nickel rich γ-phase, where the single-phase compositional range between 0 and 40 at% produced only limited scatter in the data.

It is concluded that the method of producing combinatorial Ni-Cr alloy libraries by physical vapor deposition and electron beam welding, and then rapidly characterizing the chemical and mechanical properties with EDS and nanoindentation is a suitable screening method for rapid assessment for alloy design. One sample of a nickel substrate with a chromium wedged film, one sample of a chromium substrate with a nickel wedged film, and as few as two or three welds per sample are sufficient to establish the entire composition range. If a composition range could be narrowed, then more welds could be used to produce more accurate results for alloy design or optimization.

These methods have proven successful for the combinatorial alloy design of Ni-Cr alloys, and it is assumed that similar concepts could be used in other alloy systems. Because the hardness results of the Ni-Cr system showed conclusive trends in the single-phase region, it is suggested that alloys with complete solid solutions through the entire composition be tested. An example of a suggested single solution alloy systems is Cu-Ni, where both metals have the FCC crystal structure.

The Ni-Cr alloy system was chosen because it was part of the commercially important ternary Fe-Ni-Cr alloy system. It is also suggested that the Fe-Ni and Fe-Cr binary systems are examined by these methods. Methods to establish a ternary Fe-Ni-Cr combinatorial library by similar methods should also be established. Due to the complicated phases that occur in this system, compositions closely resembling specific steels should be the focus of the work.

References

1. X.-D. Xiang, “Combinatorial Materials Synthesis and Screening: An Integrated Materials Chip Approach to Discovery and Optimization of Functional Materials”, *Annu. Rev. Mater. Sci.* 29, pp.149-171 (1999).

2. E.W. McFarland and W.H. Weinberg, “Combinatorial Approaches to Materials Discovery”, *Tibtech* 17, pp.107-115 (1999).

3. Y.-K. Yoo, F. Duewer, H. Yang, D. Yi, J.-W. Li, and X.-D. Xiang, “Room-Temperature Electronic Phase Transitions in the Continuous Phase Diagrams of Perovskite Manganites”, *Nature* 406, pp.704-708 (2000).

4. E.J. Amis, X.-D. Xiang, and J.-C. Zhao, “Combinatorial Materials Science: What’s New Since Edison?”, *MRS Bulletin*, pp. 295-300 (2002).

5. J.V. Busch, “Combinatorial Analysis- How Much Is It Worth?”, *Research-Technology Management*, pp.38-45 (2001).

6. “Technology Roadmap for Combinatorial Methods”, *Chemical Industry Vision2020 Technology Partnership*, pp. 2-8 (2001).

7. C.G. McKamey, E.P. George, C.T. Liu, J.A. Horton, C.A. Carmichael, R.L. Kennedy, and W.D. Cao, “Manufacturing of Nickel-Base Superalloys with Improved High-Temperature Performance”, *C/ORNL95-0327*, Oak Ridge National Laboratory, Oak Ridge, TN (January 2000).

8. R. Dagani, “Inorganics Go Combinatorial”, *CENEAR* 79, pp.59-63 (2001).

9. X.-D. Xiang, X. Sun, G. Briceno, Y. Lou, K.-A, Wang, H. Chang, W.G. Wallace-Freedman, S.-W. Chen, and P.G. Schultz, “A Combinatorial Approach to Materials Discovery”, *Science* 268, pp.1738-1740 (1995).

10. X.-D. Xiang, “Mapping of Physical Properties- Composition Phase Diagrams of Complex Material Systems Using Continuous Composition Material Chips”, *Applied Surface Science* 189, pp.188-195 (2002).

11. J.R. Engstrom and W.H. Weinberg, "Combinatorial Materials Science: Paradigm Shift in Materials Discovery and Optimization", *AIChE Journal* 46, pp.2-5 (2000).

12. E. Danielson, M. Devenney, D.M. Giaquinta, J.H. Golden, R.C. Haushalter, E.W. McFarland, D.M. Poojary, C.M. Reaves, W.H. Weinberg, and X.D. Wu, "A Rare-Earth Phosphor Containing One-Dimensional Chains Identified Through Combinatorial Methods", *Science* 279, pp. 837-839 (1998).

13. M.Th. Cohen-Adad, M. Gharbi, C. Goutaudier, and R. Cohen-Adad, "Melting Zone Technique as a Tool for a Combinatorial Approach in Material Science", *J. Alloys and Compounds* 289, pp.185-196 (1999).

14. M.T. Cohen-Adad, L. Laversenne, M. Gharbi, C. Goutaudler, G. Boulon, and R. Cohen-Adad, "New Combinatorial Chemistry Approach in Material Science", *J. Phase Equil.* 22, pp.379-385 (2001).

15. J.-C. Zhao, "A Combinatorial Approach for Efficient Mapping of Phase Diagrams and Properties", *J. Mater. Res.* 16, pp.1565-1578 (2001).

16. J.-C. Zhao, "A Combinatorial Approach for Structural Materials", *Adv. Eng. Mater*. 3, pp.143-147 (2001).

17. J.-C. Zhao, M.R. Jackson, and L.A. Peluso, "Determination of the Nb-Cr-Si Phase Diagram Using Diffusion Multiples", *Acta Materialia* 51, pp. 6395-6405 (2003).

18. "Heat and Corrosion Resistant Castings", *INCO Technical Bulletin*, International Nickel Company, New York, NY (1978).

19. W.F. Smith, "Structure and Properties of Engineering Alloys", *McGraw Hill Publishing*, New York, NY (1981).

20. D.R. Askeland, "The Science and Engineering of Materials (3rd edition)", *PWS Publishing*, Boston, MA (1994).

21. "4pi Revolution User Guide", found online at: <http://www.4pi.com/teksupport/Rev10online/manual/0-start.htm>.

22. W.C. Oliver and G.M. Pharr, "An Improved Method for Determining Hardness and Elastic Modulus by Load and Depth Sensing Indentation Experiments", *J. Mater. Res.* 6, pp. 1564-1583 (1992).

23. J.L. Hay and G.M. Pharr, "Instrumented Indentation Testing", *ASM Handbook Volume 8: Mechanical Testing and Evaluation* (10^{th} edition), edited by H. Kuhn and D. Medlin, ASM International, Materials Park, OH, pp. 232-243 (2000).

24. "Properties of Metals and Alloys", *Sigmund Cohn Corp.*, Mount Vernon, NY (1994).

25. R.F. Smart and F.G. Haynes, "Some Observations on the Chromium-Nickel System", *J. Institute of Metals* 91, pp.153-157 (1962).

26. J.S. Ogborn, D.L. Olson, and M.J. Cieslak, "Influence of Solidification on the Microstructural Evolution of Nickel Base Weld Metal", *Mat. Sci. & Eng.* A203, pp. 134-139 (1995).

27. T. Umeda and T. Okane, "Solidification MicrostructuresSelection of Fe-Cr-Ni and Fe-Ni Alloys", *Sci. & Tech. Of Adv. Mat.* 2, pp. 231-240 (2001).

28. P.G. Schultz and X.-D Xiang, "Combinatorial Approaches to Materials Science", *Current Opinion in Solid State & Materials Science* 3, pp.153-158 (1998).

29. X.-D Xiang and P.G. Schultz, "The Combinatorial Synthesis and Evaluation of Functional Materials", *Physica C* 282-287, pp.428-430 (1997).

30. Y.K. Yoo and X.-D. Xiang, "Combinatorial Material Preparation", *J. Phys.: Condens. Matter* 14, pp.49-78 (2002).

31. R.B. van Dover, L.F. Schneemeyer, and R.M. Fleming, “Discovery of a Useful Thin-Film Dielectric Using a Composition-Spread Approach”, *Nature* 392, pp.162-164 (1998).

32. B. Jandeleit, D.J. Schaefer, T.S. Powers, H.W. Turner, and W.H. Weinberg, “Combinatorial Materials Science and Catalysis”, *Angew. Chem. Ed.* 38, pp.2494-2532 (1999).

33. R. Cremer and S. Richter, “Rapid Chemical and Structural Characterization of Metastable Thin-Film Libraries by a Combination of Electron Probe Microanalysis and Scanning X-Ray Diffraction”, *Surface Interface Analysis* 34, pp.686-689 (2002).

34. Y.R. de Miguel, “What Next in Combinatorial Chemistry?”, *Tibtech* 18, pp.43-44 (2000).

35. S. Kimura, “Prospect of Materials Research Methodology by Combinatorial Approach”, *Applied Surface Science* 189, pp.177-178 (2002).

36. R.F. Service, “Combinatorial Chemistry: High-Speed Materials Design”, *Science* 277, pp.474-475 (1997).

37. J.D. Hewes and L.A. Bendersky, “High Throughput Materials Research and Development: A Growing Effort at NIST”, *Applied Surface Science* 189, pp.196-204 (2002).

38. S.E. Russek, W.E. Bailey, G. Alers, and D.L. Abraham, “Magnetic Combinatorial Thin-Film Libraries”, *IEEE Transactions on Magnetics* 37, pp.2156-2158 (2001).

39. J.A. Kittl, P.G. Sanders, M.J. Aziz, D.P. Brunco, and M.O. Thompson, “Complete Experimental Test of Kinetic Models for Rapid Alloy Solidification”, *Acta Mater* 48, pp.4797-4811 (2000).

40. Y.K. Yoo, T. Ohnishi, G. Wang, F. Duewer, X.-D Xiang, Y.S. Chu, D.C. Mancini, Y.-Q. Li, and R.C. O'Handley, "Continuous Mapping of Structure-Property Relations in $Fe_{1-x}Ni_x$ Metallic Alloys Fabricated by Combinatorial Synthesis", *Intermetallics* 9, pp.541-545 (2001).

41. R.W. Cahn, "Materials Science: Rapid Alloy Assessment", *Nature* 410, pp.643-644 (2001).

42. R. Cremer and D. Neuschütz, "A Combinatorial Approach to the Optimization of Metastable Multicomponent Hard Coatings", *Surface and Coatings Technology* 146-147, pp.229-236 (2001).

43. H. Koinuma, H.N. Aiyer, and Y. Matsumoto, "Combinatorial Solid State Materials Science and Technology", *Science and Technology of Advanced Materials* 1, pp.1-10 (2000).

44. C. Daniel, F. Mucklich, and Z. Liu, "Periodical Micro-Nano-Structuring of Metallic Surfaces by Interfering Laser Beams", *Applied Surface Science* 208-209, pp.317-321 (2003).

45. R. Cremer, K. Reichert, and D. Neuschütz, "A Composition Spread to the Optimaization of (Ti,Al)N Hard Coatings Deposited by DC and Bipolar Pulsed Magnetron Sputtering", *Surface and Coatings Technology* 142-144, pp.642-648 (2001).

46. G. Briceño, H. Chang, X. Sun, P.G. Schultz, and X.-D. Xiang, "A Class of Cobalt Oxide Magnetoresistance Materials Discovered with Combinatorial Synthesis", *Science* 270, pp.273-275 (1995).

47. Mattox, D.M., "Handbook of Physical Vapor Deposition (PVD) Processing", *Noyes Publications*, Westwood, NJ (1998).

48. M.M. Mohebi and J.R.G. Evans, "A Drop-on-Demand Ink-Jet Printer for Combinatorial Libraries and Functionally Graded Ceramics", *J. Comb. Chem.* 4, pp.267-274 (2002).

49. E.D. Specht, A. Rar, G.M. Pharr, E.P. George, P. Zschack, H. Hong, and J. Ilavsky, “Rapid Structural and Chemical Characterization of Ternary Phase Diagrams Using Synchrotron Radiation”, *J. Mat. Res.*, pp. 2522-2527 (2003).

50. G.E. Ice and B.C. Larson, “3D X-Ray Crystal Microscope”, *Adv. Eng. Mater.* 2, pp. 643-646 (2000).

51. E. Reddington, A. Sapienza, B. Gurau, R. Viswanathan, S. Sarangapani, E.S. Smotkin, and T.E. Mallouk, “Combinatorial Electrochemistry: A Highly Parallel, Optical Screening Method for Discovery of Better Electrocatalysts”, *Science* 280, pp. 1735-1737 (1998).

Vita

Jaret James Frafjord was born in Moscow, ID on October 11, 1979. He was raised in West Richland, WA and graduated with honors from Hanford High School in June 1998. From there he enrolled at the University of Idaho and earned a Bachelor of Science degree in metallurgical engineering in May 2002.

After graduation, he moved across the country and enrolled in the graduate program at the University of Tennessee-Knoxville under the direction of Dr. George Pharr. Jaret was able to conduct the majority of his graduate research at Oak Ridge National Laboratory, which helped him to earn his Masters of Science degree in materials science and engineering in December 2004.

Jaret is currently working as a physical testing engineer for BWXT Y-12 at the Y-12 National Security Complex in Oak Ridge, TN.